Uncertainty in the Winter Tropospheric Response to Arctic Sea Ice Loss: The Role of Stratospheric Polar Vortex Internal Variability

LANTAO SUN,[a] CLARA DESER,[b] ISLA SIMPSON,[b] AND MICHAEL SIGMOND[c]

[a] *Department of Atmospheric Science, Colorado State University, Fort Collins, Colorado*
[b] *Climate and Global Dynamics, National Center for Atmospheric Research, Boulder, Colorado*
[c] *Canadian Centre for Climate Modelling and Analysis, Environment and Climate Change Canada, Victoria, British Columbia, Canada*

(Manuscript received 16 July 2021, in final form 21 December 2021)

ABSTRACT: Arctic sea ice has declined rapidly over the past four decades and climate models project a seasonally ice-free Arctic Ocean by the middle of this century, with attendant consequences for regional climate. However, modeling studies lack consensus on how the large-scale atmospheric circulation will respond to Arctic sea ice loss. In this study, the authors conduct a series of 200-member ensemble experiments with the Community Atmosphere Model version 6 (CAM6) to isolate the atmospheric response to past and future sea ice loss following the Polar Amplification Model Intercomparison Project (PAMIP) protocol. They find that the stratospheric polar vortex response is small compared to internal variability, which in turn influences the signal-to-noise ratio of the wintertime tropospheric circulation response to ice loss. In particular, a strong (weak) stratospheric polar vortex induces a positive (negative) tropospheric northern annular mode (and North Atlantic Oscillation), obscuring the forced component of the tropospheric response, even in 100-member averages. Stratospheric internal variability is closely tied to upward wave propagation from the troposphere and can be explained by linear wave interference between the anomalous and climatological planetary waves. Implications for the detection of recent observed trends and model realism are also presented. These results highlight the inherent uncertainty of the large-scale tropospheric circulation response to Arctic sea ice loss arising from stratospheric internal variability.

KEYWORDS: Arctic; Sea ice; Uncertainty; Stratosphere-troposphere coupling; Climate models; Internal variability

1. Introduction

Arctic sea ice has declined rapidly over the past four decades (Fetterer et al. 2017) and the vast majority of climate models participating in phase 6 of the Coupled Model Intercomparison Project (CMIP6) project a seasonally ice-free Arctic Ocean by 2050 in all emission scenarios (Notz et al. 2020). The loss of sea ice and its consequences for the global climate system are one of the grand science challenges of the World Climate Research Programme (WCRP). Sea ice loss causes near-surface warming and increased precipitation at high latitudes, especially in winter (e.g., Screen and Simmonds 2010; Deser et al. 2010), due to enhanced upward fluxes of heat and moisture from the ocean to the atmosphere. The remote response, however, is more complex in its physical mechanisms, and there is less consensus among different studies (e.g., Cohen et al. 2020). In particular, whether observed Arctic sea ice loss has contributed to colder winters over North America and Eurasia in recent decades remains a topic of extensive debate (Overland et al. 2011; Cohen et al. 2013; Mori et al. 2014; Perlwitz et al. 2015; McCusker et al. 2016; Sun et al. 2016; Ogawa et al. 2018; Blackport et al. 2019; Dai and Song 2020), highlighting the challenge of distinguishing the sea ice loss effect from internal variability and the incomplete mechanistic understanding of the underlying processes (Barnes and Screen 2015).

Previous modeling studies have revealed aspects of the dynamical mechanisms connecting Arctic sea ice loss to large-scale atmospheric circulation changes. For example, Deser et al. (2004) suggested there is a direct and an indirect component of the winter atmospheric circulation response to Arctic sea ice loss. The direct component is localized to the vicinity of the ice loss region and exhibits a baroclinic structure in the vertical with a surface trough and upper-level ridge. The indirect component is hemispheric in scale and barotropic in the vertical throughout the troposphere, resembling the northern annular mode (NAM; Thompson and Wallace 2000) or North Atlantic Oscillation (NAO; Hurrell 1995). More recently, it has been argued that Arctic sea ice loss can also cause a weakening of the stratospheric polar vortex, which subsequently induces a negative phase of the tropospheric NAM/NAO in late winter (Peings and Magnusdottir 2014; Kim et al. 2014; Sun et al. 2015). This "stratospheric pathway" is distinct from the "tropospheric pathway" [i.e., that presented in Deser et al. (2004)] and has been suggested to play a dominant role in the inferred atmospheric circulation response to observed sea ice loss in the Barents–Kara Seas (Jaiser et al. 2013; Wu and Smith 2016; Nakamura et al. 2016; Zhang et al. 2017, 2018). It is also consistent with the observed increased frequency of January–February weak polar vortex states in recent decades (Kretschmer et al. 2018). However, the stratospheric response to autumn sea ice loss and its subsequent influence on the wintertime tropospheric response was found to be small compared to the concurrent effect of winter ice loss (Sun et al.

Supplemental information related to this paper is available at the Journals Online website: https://doi.org/10.1175/JCLI-D-21-0543.s1.

Corresponding author: Lantao Sun, lantao.sun@colostate.edu

DOI: 10.1175/JCLI-D-21-0543.1

2015; Blackport and Screen 2019). Moreover, atmospheric models forced with observed or projected future Arctic sea ice loss simulate a range of stratospheric polar vortex responses, including weakening (Kim et al. 2014; Nakamura et al. 2016), strengthening (Cai et al. 2012; Scinocca et al. 2009; Screen et al. 2013; Sun et al. 2014; England et al. 2018), and no change (Dai and Song 2020). This range of responses may have many contributing factors, including structural differences among models in their representation of the mean state (Smith et al. 2017) and eddy–mean flow feedbacks (e.g., Smith et al. 2022), differences in the regional patterns of imposed sea ice loss (Peings and Magnusdottir 2014; Sun et al. 2015; McKenna et al. 2018; Screen 2017), and inadequate sampling of internal variability that obscures the forced response (Seviour 2017). Without modeling consensus, it is difficult to interpret observed relationships between sea ice loss and winter atmospheric circulation (e.g., ice loss in the Barents–Kara Seas and NAO: Peings 2019; Warner et al. 2020).

To account for the sources of divergent stratospheric and tropospheric responses among different studies, there is an urgent need for coordinated model experiments. The CMIP6 Polar Amplification Model Intercomparison Project (PAMIP) aims to investigate the causes and consequences of polar amplification through a coordinated set of numerical model experiments (Smith et al. 2019). So far, early comparisons have been conducted to address the robustness of sea ice–induced atmospheric circulation change and its underlying mechanisms (Ronalds et al. 2020; Smith et al. 2022).

As mentioned above, the low signal-to-noise ratio is one major obstacle for the detection of an atmospheric circulation response to Arctic sea ice loss (Liang et al. 2020). While some common features of the atmospheric response to projected late-twenty-first-century Arctic sea ice loss have been found across models (Screen et al. 2018; Hay et al. 2018, 2022), there are substantial discrepancies among modeling studies that consider the response to observed (and thus weaker) Arctic sea ice loss (e.g., Screen et al. 2014). In particular, Sun et al. (2018) investigated the atmospheric circulation response to transient sea ice change from 1990 to 2090 and found that the forced signal is small compared to the noise from internal variability, especially in the early decades when the ice loss is more limited. To better isolate the signal, a useful approach is to use large ensembles of simulations so as to reduce the noise, in analogy with the initial-condition large ensemble framework used in climate change studies (Kay et al. 2015; Maher et al. 2019; Deser et al. 2020). In particular, the minimum ensemble size needed to detect a statistically significant atmospheric circulation response signal was found to exceed 50 in the case of observed Arctic sea ice loss (Screen et al. 2014) and 200 according to newer calculations (Labe 2020).

More recently, Peings et al. (2021, hereafter P21) examined the atmospheric circulation response to future-minus-preindustrial Arctic sea ice loss based on simulations following the PAMIP time-slice protocol with uncoupled and coupled versions of Specified Chemistry–Whole Atmosphere Community Climate Model version 4 (SC-WACCM4) and found significant inconsistencies among three discrete 100-member ensembles. They identified tropospheric dynamics and ENSO-induced teleconnections as the main sources of internal variability leading to the inconsistencies.

This study utilizes the PAMIP time-slice simulations with Community Atmosphere Model version 6 (CAM6) to investigate the effect of Arctic sea ice loss from the preindustrial period to the present day, and from the present day to the mid-twenty-first century, under two different background SST states. Our study differs from P21 in the following ways. First, we explore role of stratospheric internal variability in the tropospheric response to past and future Arctic sea ice loss, whereas P21 focused on the role of tropospheric internal variability in the response to mid-twenty-first-century minus preindustrial sea ice loss under a single background SST state. Second, we go beyond the discrete case study approach of P21 by conducting a random sampling bootstrapping procedure to more robustly quantify the spread in tropospheric circulation responses to Arctic sea ice loss arising from internal variability. Third, while P21 and our results both suggest that it is challenging to make causal inferences based on analysis of observations alone due to confounding of internal variability in short (<50 years) records, our results explicitly highlight the stratospheric pathway, which has received much attention in the observational literature.

The rest of this paper is organized as follows. Section 2 contains a description of the model and the PAMIP experimental protocol. Section 3 presents results on the relative magnitudes of the stratospheric response to Arctic sea ice loss versus internal variability, the influence of stratospheric internal variability on the tropospheric response to sea ice loss, and its mechanism. Section 4 discusses the implications for detection of recent observed trends and model realism. A summary and discussion follow in section 5.

2. Model and experimental design

a. *Model description*

CAM6 is the atmospheric model component of Community Earth System Model 2 (CESM2) developed at the National Center for Atmospheric Research (NCAR). It uses the same finite-volume (FV) dynamical core as previous versions, but includes the unified turbulence scheme "Cloud Layers Unified by Binormals" (CLUBB; Larson 2017) as well as updates to almost all of the parameterizations (Danabasoglu et al. 2020). CAM6 ranks within the top 10% of the CMIP6 models in representing many features of the atmospheric circulation such as storm tracks, stationary waves, and blocking (Simpson et al. 2020). CAM6 has a horizontal resolution of 1.25° in longitude and 0.9° in latitude, and 32 vertical levels with the model top at 2.26 hPa (Danabasoglu et al. 2020). As a "low-top" model, it does not generate a quasi-biennial oscillation (QBO). The sudden stratospheric warming frequency in CAM6 is also underestimated (Ayarzagüena et al. 2020), likely resulting from a too-strong mean polar vortex. However, as we shall show, the interannual variability of the stratospheric polar vortex and its downward influence on the troposphere are generally realistic.

TABLE 1. PAMIP atmosphere-only time-slice experiments conducted in this study using Community Atmosphere Model version 6 (see text for details of the experimental design). Nomenclature follows that in Smith et al. (2019).

No.	Expt name	SST forcing	SIC forcing	Other details
1.1	pdSST-pdSIC	Present-day conditions	Present-day conditions	
1.2	piSST-piSIC	Preindustrial conditions	Preindustrial conditions	
1.3	piSST-pdSIC	Preindustrial conditions	Present-day conditions	Year 2000 radiative forcing; 14-month time-slice run with the first 2 months discarded as spinup; ensemble size of 200; set ice thickness set to be 2 m in the Arctic and 1 m in the Antarctic
1.4	futSST-pdSIC	Future conditions	Present-day conditions	
1.5	pdSST-piArcSIC	Present-day conditions	Preindustrial conditions in the Arctic, present-day conditions in the Antarctic	
1.6	pdSST-futArcSIC	Present-day conditions	Future conditions in the Arctic, present-day conditions in the Antarctic	
	futSST-futArcSIC	Future conditions	Future conditions in the Arctic, present-day conditions in the Antarctic	

b. PAMIP experimental protocol

We conduct atmosphere-only time slice experiments following PAMIP protocols. In these experiments, the radiative forcing is fixed at year 2000, and sea surface temperatures (SST) and sea ice concentrations (SIC) are prescribed at preindustrial (pi), present-day (pd), and future (fut) conditions (Smith et al. 2019). The pd SST and SIC are taken from observations, while the pi and fut lower boundary forcings are constructed from the 31 historical and representative concentration pathway 8.5 (RCP8.5) simulations respectively from the corresponding 31 models from phase 5 of the Coupled Model Intercomparison Project (CMIP5) (Smith et al. 2019). For each ensemble member, the pi period is defined as the 30 years when the global mean temperature (GMT) equals 13.67°C, obtained by removing an estimated global warming index (Haustein et al. 2017) of 0.57°C from the observed 1979–2008 value (14.24°C). The fut period is defined as the 30 years when the GMT first exceeds the pi GMT by +2°C, typically near 2030–60 (Hausfather 2020). Thus, the magnitude of the sea ice loss from pd to fut prescribed in PAMIP is substantially smaller than the end-of-twenty-first-century ice loss commonly used in previous studies (e.g., Screen et al. 2018). The sea ice thickness is set to be uniformly 2 m in the Arctic and 1 m in the Antarctic.

Here we conduct the following PAMIP experiments [nomenclature follows that in Table 1 of Smith et al. (2019)]: 1.1: pdSST-pdSIC; 1.2: piSST-piSIC; 1.3: piSST-pdSIC; 1.4: futSST-pdSIC; 1.5: pdSST-piArcSIC; and 1.6: pdSST-futArcSIC (note that for 1.5 and 1.6, pd SIC is prescribed in the Antarctic). We also conduct an additional experiment: futSST-futArcSIC (with pd SIC prescribed in the Antarctic). Each simulation starts on 1 April 2000, initialized from ensemble member 001 of the CAM6 Atmospheric Model Intercomparison Project (AMIP) historical simulation, and runs for 14 months; we discard the first 2 months as spinup from our analysis. For each experiment, we conduct a 200-member ensemble using the method of "pertlim" [an order 10^{-14} K perturbation to the initial atmospheric temperature field following Kay et al. (2015)]. Additional details of the PAMIP protocols and the SST/SIC forcing can be found in Table 1 and in Smith et al. (2019).

We calculate the atmospheric response to past (pdSIC minus piSIC: Δpast) and future (futSIC minus pdSIC: Δfut) Arctic sea ice loss from the 200-member ensemble means of each experiment as follows:

$$\Delta\text{past}_{\text{piSST}} = 1.3\ (\text{piSST-pdSIC}) - 1.2\ (\text{piSST-piSIC}), \quad (1)$$

$$\Delta\text{past}_{\text{pdSST}} = 1.1\ (\text{pdSST-pdSIC}) - 1.5\ (\text{pdSST-piArcSIC}), \quad (2)$$

$$\Delta\text{fut}_{\text{pdSST}} = 1.6\ (\text{pdSST-futArcSIC}) - 1.1\ (\text{pdSST-pdSIC}), \quad (3)$$

$$\Delta\text{fut}_{\text{futSST}} = (\text{futSST-futArcSIC}) - 1.4\ (\text{futSST-pdSIC}). \quad (4)$$

Note that there are two background SST states for the atmospheric circulation responses to both past and future Arctic sea ice loss. This allows us to investigate whether the responses are sensitive to the background SST state (e.g., Smith et al. 2017). The false discovery rate (FDR) with control level $\alpha_{\text{FDR}} = 0.2$ has been applied to the 90% statistical significance level on the two-sided Student's t test to measure the field significance of the responses (Wilks 2016).

c. Random sampling procedure

The PAMIP protocol recommends a minimum ensemble size of 100 members (Smith et al. 2019). We therefore begin our investigation by examining the sensitivity of the results based on the first 100 members and the second 100 members of our 200-member Δpast and Δfut ensembles, similar to P21's approach. The marked differences between these two independent 100-member subensembles leads us to then conduct a more systematic assessment of sampling uncertainty due to internal variability using a random sampling (bootstrapping) procedure (Mudelsee 2010). For each Δpast and Δfut ensemble, we randomly selected 100 members with replacement from the full 200 members, computed the average of each random 100-member subset, and repeated the entire procedure 1000 times. We then used these 1000 random 100-member averages to compute a probability distribution function (PDF) for each of the Δpast and Δfut ensembles.

d. Characterizing stratospheric internal variability

Following convention, we define an index of the strength of the winter [December–February average (DJF)] stratospheric polar vortex as the zonal-mean zonal wind at 10 hPa and 60°N (hereafter, U10). We compute U10 for each of the 1000 bootstrapped samples of 100-member averages, and use these to compute PDFs. We also calculate analytical PDFs of 100-member averages of U10 for each of the Δpast and Δfut ensembles, assuming a Gaussian distribution with mean X_N (equal to the 200-member average) and a standard deviation σ_N:

$$\sigma_N = \sigma\sqrt{\frac{2}{N}}, \tag{5}$$

where σ is the standard deviation of U10 across the original 200 members of each ensemble and $N = 100$. The factor of $\sqrt{2}$ accounts for the fact that we are calculating the standard deviation of the difference between a pair of simulations. As shown in section 3b, the two approaches generate very similar PDFs. Finally, we compute correlation and regression coefficients between U10 and other quantities of interest across the 1000 bootstrapped samples of 100-member averages.

3. Results

a. Surface atmospheric response to past and future Arctic sea ice loss

The loss of Arctic SIC (%) prescribed in the Δpast and Δfut ensembles occurs mainly within the central Arctic in summer and autumn, and in the marginal ice zones (e.g., Sea of Okhotsk, Bering Sea, and Labrador Sea) in winter and spring (Fig. 1a). In the Δfut ensemble, the SIC reduction in summer and autumn extends all the way to the North Pole (Fig. 1a), with a corresponding increase (up to 140%) in the areal extent of ice loss from July to December compared to the Δpast ensemble (Fig. 1b). The loss of Arctic SIC (%) prescribed in the Δpast and Δfut ensembles shares regional and seasonal characteristics with observed SIC trends since 1979 (Fig. S1 in the online supplemental material).

Sea ice loss results in a net upward energy flux from the ocean to the atmosphere, which in turn is responsible for the near-surface warming over the Arctic and high-latitude continents, as well as the increase in Arctic precipitation (Fig. 2). These responses exhibit similar seasonal cycles, with a minimum in summer and a maximum in winter; note the roughly 2-month delay between the peak sea ice loss (October) and the largest atmospheric response (December) for the future ice loss case, in agreement with previous studies (e.g., Deser et al. 2010). The winter surface energy flux and temperature/precipitation responses are approximately twice as large for future ice loss compared to past ice loss, in keeping with the relative magnitudes of sea ice reduction, and show little sensitivity to the background SST conditions, especially for the past ice loss case (Fig. 2). The slightly weaker (~10%) but statistically significant responses for the future ice loss case under future SSTs compared to present-day SSTs is most apparent in October–December (Fig. 2 and Fig. S2). It is likely related to enhanced poleward atmospheric energy transport, which warms the Arctic free troposphere (Audette et al. 2021), thus reducing the upward energy transfer from the ocean surface. Outside the Arctic, the atmospheric responses to the same Arctic sea ice loss but under different background SST conditions are largely indistinguishable (not shown). Moreover, internal variability of the surface energy flux response based on 100-member averages is relatively small and thus may not contribute much to the spread in atmospheric response (see error bars in top panel of Fig. 2). In the remainder of this study, we focus on the winter season when the atmospheric response is largest.

b. Stratospheric internal variability and its influence on the tropospheric response

To demonstrate the relative magnitudes of the mean stratospheric response to Arctic sea ice loss and its internal variability based on 100-member averages, we show PDFs of the 1000 U10 bootstrapped samples (histograms) along with the analytical distribution (thick black curves) for each of the four ice loss cases in DJF (Fig. 3). The mean U10 response of the 1000 100-member averages is −1.6, −0.7, −0.4, and +0.5 m s^{-1} for $\Delta\text{past}_{\text{piSST}}$, $\Delta\text{past}_{\text{pdSST}}$, $\Delta\text{fut}_{\text{pdSST}}$, and $\Delta\text{fut}_{\text{futSST}}$, respectively. The difference in U10 responses between the two SST states is statistically insignificant for both Δpast and Δfut. In comparison, the standard deviation of the thousand 100-member averages ranges from 1.4 to 1.6 m s^{-1} (similar values obtain for the analytical solution) for all four sea ice cases, indicating a low signal-to-noise ratio for 100-member averages. Due to the low signal-to-noise, by chance, the first and second 100-member averages of U10 (e.g., members 1–100 and 101–200) can differ significantly, as is the case for $\Delta\text{past}_{\text{piSST}}$ (~−5.2 vs 1.9 m s^{-1}) and $\Delta\text{fut}_{\text{pdSST}}$ (~−3.0 vs 2.3 m s^{-1}), or be nearly indistinguishable, as is the case for $\Delta\text{past}_{\text{pdSST}}$ (−0.9 vs −0.4 m s^{-1}) and $\Delta\text{fut}_{\text{pdSST}}$ (0.5 vs 0.5 m s^{-1}).[1] Since the four sea ice cases have very similar magnitudes of internal variability, these differences highlight the importance of assessing the full distribution via random subsampling rather than relying on two discrete (albeit fully independent) estimates. Indeed, the first and second 100-member averages of U10 for $\Delta\text{past}_{\text{piSST}}$ slightly exceed two standard deviations of the PDF, indicating that they are low probability occurrences. Below, we use this case ($\Delta\text{past}_{\text{piSST}}$) as an example to illustrate how the random sampling of internal stratospheric variability in any 100-member average affects the apparent tropospheric response to Arctic sea ice loss.

The vertical structure of the DJF zonal-mean zonal wind response in $\Delta\text{past}_{\text{piSST}}$ based on the full 200-member average shows a statistically significant deceleration of the mean

[1] It is noted that there is a very low probability that two of the four cases show significant differences between the first and second 100-member averages. We have exhaustively checked that there were no other underlying reasons for this, and put it down to chance.

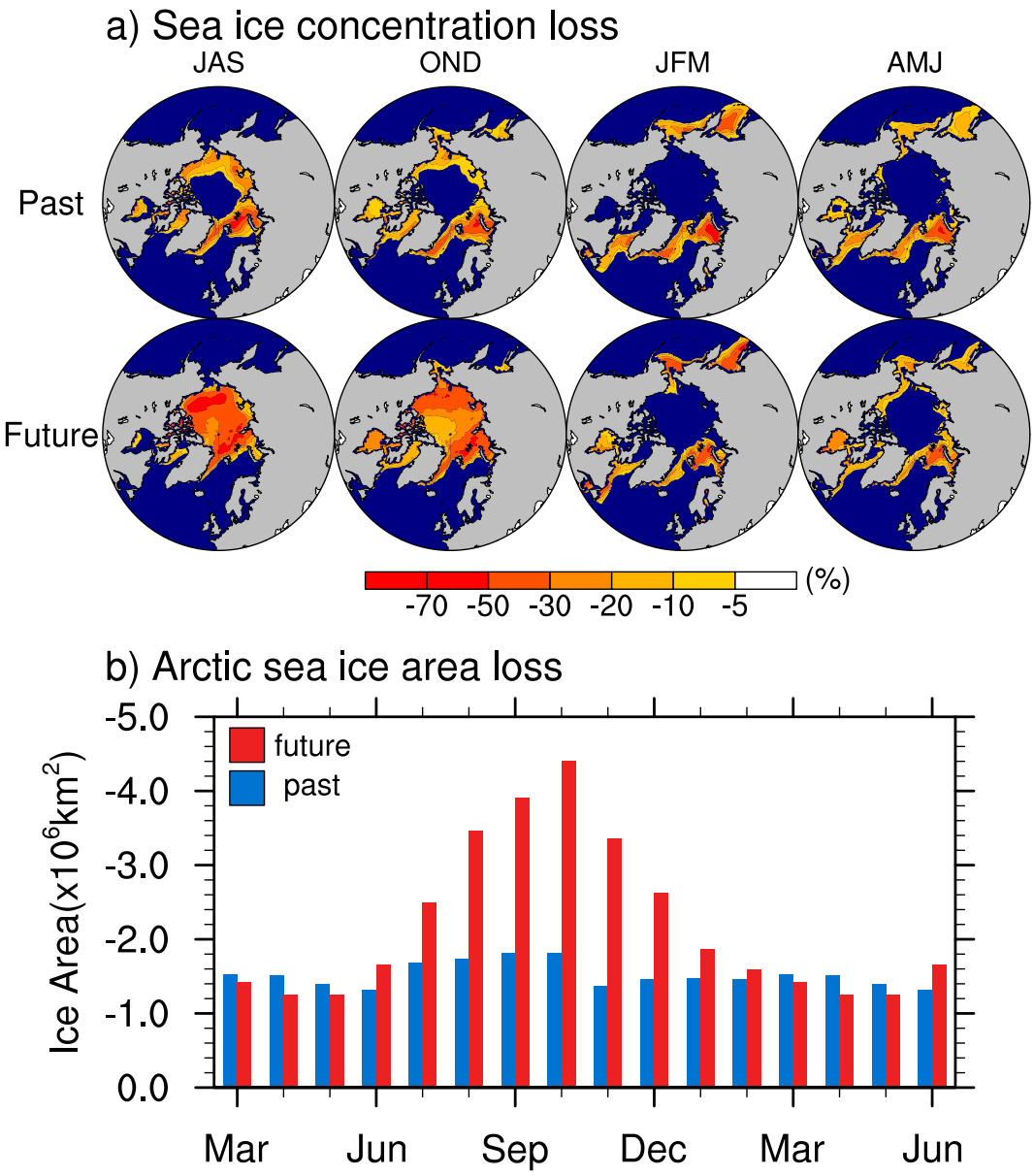

FIG. 1. (a) Seasonal maps of prescribed Arctic SIC loss (%) in the PAMIP experiments for the past (preindustrial to present day) and future (present day to +2°C warming above preindustrial level). Summer, autumn, winter, and spring seasons are defined to be the average of July–September (JAS), October–December (OND), January–March (JFM), and April–June (AMJ), respectively. (b) Monthly Arctic sea ice area loss (10^6 km^2) for the past (blue) and future (red); note the inverted *y*-axis scale.

westerlies throughout the troposphere and stratosphere at high latitudes (60°–80°N; maximum values around -2.5 m s^{-1} at 10 hPa), and very little response equatorward of 50°N (Fig. 4a). Inspection of the first and second 100-member averages reveals striking differences in both the stratosphere and troposphere. The polar vortex weakens substantially in the first 100 members but strengthens in the second 100 members, albeit not significantly (Figs. 4b,c). The tropospheric circulation response in the first 100-member average shows a meridional dipole with deceleration (acceleration) centered at 60°N (35°N), resembling the full 200-member average but with larger magnitudes. By contrast, the second 100-member average lacks any statistically significant signal in the extratropical troposphere. These results indicate that using two discrete and independent estimates can lead to nonrobustness of atmospheric circulation responses to past and future Arctic sea ice loss in the PAMIP experiments when based on 100 members.

It is well known that the NH stratospheric polar vortex is dynamically coupled to the troposphere in boreal winter (e.g., Baldwin et al. 2021). Given that the differences between the

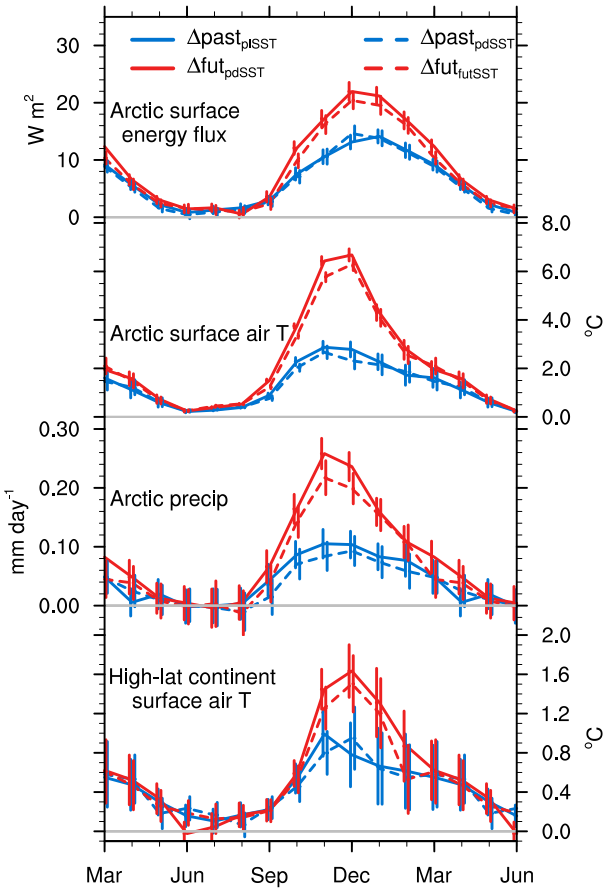

FIG. 2. Monthly responses to past (blue) and future (red) Arctic sea ice loss for (from top to bottom) Arctic net upward surface energy flux (W m^{-2}; positive upward), Arctic surface air temperature (°C), Arctic precipitation (mm day^{-1}), and high-latitude (poleward of 50°N) terrestrial surface air temperature (°C). The surface energy flux is the sum of the turbulent (sensible plus latent) heat flux and the longwave radiative flux. Solid and dashed blue curves indicate the past sea ice loss with preindustrial and present-day background SSTs, while solid and dashed red curves indicate the future sea ice loss with present-day and future background SSTs. The Arctic responses are averaged over all grid boxes containing a minimum of 15% present-day climatological SIC in March. Vertical line segments show the two standard deviation error bars based on the bootstrapped 100-member averages (see text for details).

first and second 100-member averages span the stratosphere and troposphere, one may surmise that there is a connection between the internal variability in the two domains. To examine this, we plot the monthly evolution of $U(z)$ at 60°N (a proxy for the NAM; Butler et al. 2017) for the first and second 100-member averages and their difference (Figs. 5a–c). Notably, $U(z)$ shows a distinct evolution in the two 100-member averages, consistent with Fig. 4, and their difference is characterized by maximum easterly anomalies peaking in January/February in the stratosphere and February/March at the surface, suggestive of a downward influence.

To further explore stratosphere–troposphere coupling more generally, we regress the monthly $U(z)$ response at 60°N onto the normalized DJF U10 response across the 1000 bootstrapped samples of 100-member averages. We then add or subtract the regression coefficients (multiplied by 2) to the 200-member average to form the 2.5th–97.5th-percentile confidence intervals on the mean response based on 100-member averages (Figs. 5d,e). The results based on regression analysis bear a striking resemblance to the first and second 100-member averages, indicating that most of the difference between the first and second 100-member averages arises from a random, albeit extreme, sampling of stratospheric polar vortex internal variability. Using Pearson correlations in place of regressions reveals a strong connection (r = 0.5–0.6) between DJF U10 and near-surface U response in January, February, and March, lending further support to the conjecture that stratospheric internal variability exerts a substantial influence on the troposphere (Fig. 5g).

Figure 6 shows the Δpast$_{piSST}$ geopotential height response in the stratosphere (10 hPa in DJF) and troposphere [500, 850, and 1000 hPa in January–March (JFM)] for the first and second 100-member averages and their difference. Consistent with Figs. 4 and 5, the winter polar vortex weakens (consistent with a positive geopotential height anomaly) in the first 100 members but strengthens (consistent with a negative geopotential height anomaly) in the second 100 members. In the troposphere, the first 100-member average shows a barotropic pattern with positive height anomalies over the Arctic and negative height anomalies over North Atlantic midlatitudes, projecting onto the negative phase of the NAO. By contrast, the second 100-member average exhibits a more baroclinic vertical structure in the Nordic seas, with a negative anomaly near the surface and positive anomaly in the upper levels, similar to the direct response in Deser et al. (2004). The circulation response in the North Pacific is also opposite between the two 100-member averages.

Figure 7 shows the corresponding regression maps between U10 and geopotential height based on the 1000 bootstrapped samples of 100-member averages. The patterns in the Mean + 2σ and Mean − 2σ regression maps are largely similar to the first and second 100-member averages, respectively, except over the lower-latitude North Pacific (20°–40°N). In this region, the difference between the two 100-member averages shows an anomalous ridge that is absent from the regression pattern (Figs. 6c and 7c). In addition, the anomalous trough over the North Atlantic extends farther into the Mediterranean Sea in the regression pattern compared to the difference between two subensembles. Overall, the regression pattern (Fig. 7c) closely resembles the NAM throughout the depth of the troposphere, while the difference between the two subensembles exhibits additional regional features (Fig. 6c). The magnitude of the correlation coefficients between U10 and geopotential height across the bootstrapped samples exceeds 0.9 at 10 hPa and reaches 0.6 in the troposphere over the main centers of action of the NAM (Fig. S3). Taken together, the results shown in Figs. 5–7 indicate that internal variability of the stratospheric polar vortex exhibits a strong connection to the tropospheric NAM, but that the troposphere also contains its own intrinsic modes of variability.

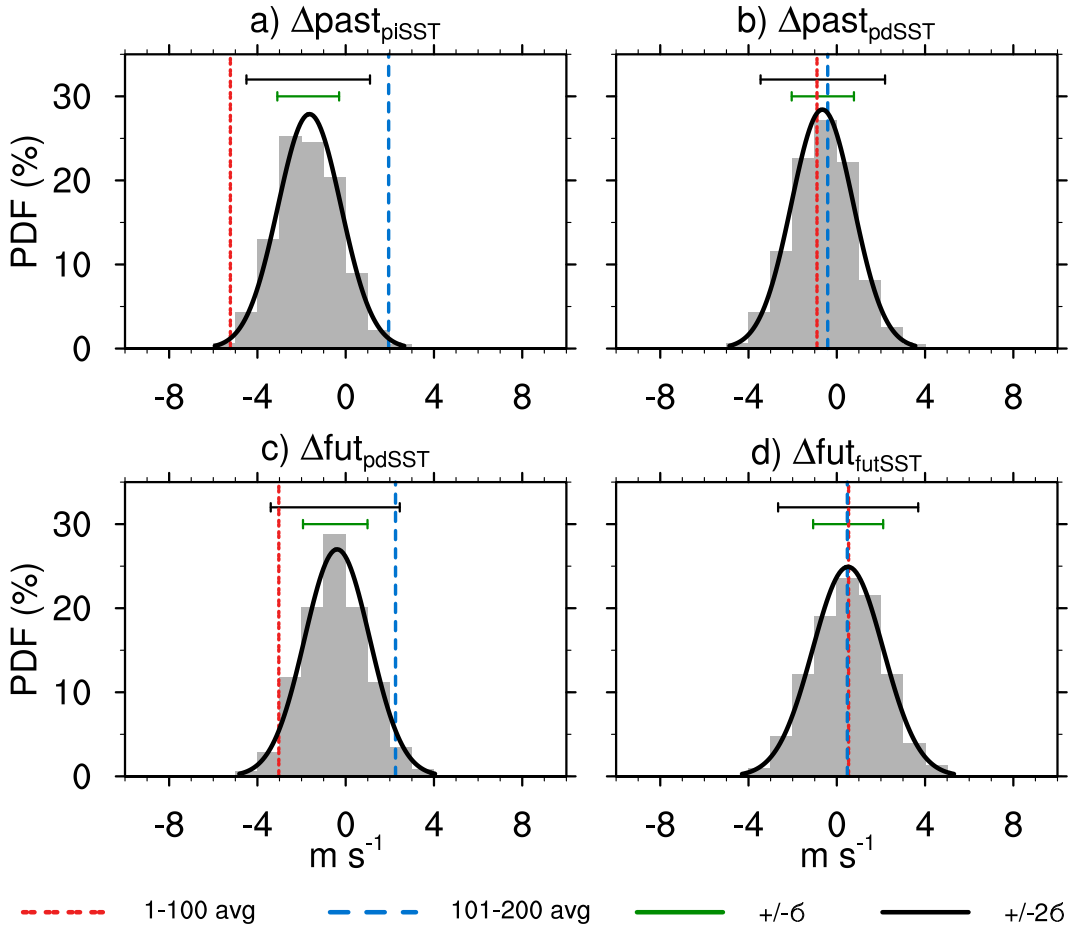

FIG. 3. Probability density function (PDF) of 100-member averages of DJF U10 for (a) $\Delta past_{piSST}$, (b) $\Delta past_{pdSST}$, (c) Δfut_{pdSST}, and (d) Δfut_{futSST}. For each case, the histogram is evaluated by randomly selecting 100 members with replacement from the 200-member ensembles and repeating this procedure 1000 times. Curves are calculated analytically from the interannual standard deviation (see text). Horizontal green (black) bar indicates plus and minus one (two) standard deviations of the PDF. Vertical dashed red (blue) line indicates the average over the first (second) 100 members.

Stratospheric internal variability can also introduce uncertainty in the surface climate response to Arctic sea ice loss estimated from 100-member averages. For example, the pattern and amplitude of the surface air temperature (SAT) response in JFM shows striking differences between the two subensembles of $\Delta past_{piSST}$ (Figs. 8a,b; shading). In particular, the second 100-member average exhibits strong and statistically significant warming over northern Eurasia (maximum values exceeding 1.5°C over eastern Siberia), whereas the first 100-member average shows weak and statistically insignificant anomalies of both signs in this region. Notable differences in warming amplitude between the two subensembles are also found over Greenland and northeastern Canada. These SAT differences are clearly linked to the different circulation responses in the two subensembles noted earlier, in particular the opposing SLP responses over the Arctic (contours in Figs. 8a,b). Indeed, the difference between the two subensembles shows evidence of dynamically induced cooling over northern Eurasia, and warming over eastern Canada and Greenland, in association with the negative NAM-like SLP pattern (Fig. 8c). The regression analysis based on U10 (Mean $-$ 2σ and Mean + 2σ; Figs. 8d,e) reproduces almost all of the SAT and SLP features seen in the two subensembles, and the difference pattern (Fig. 8f) shows the canonical SAT and SLP signatures associated with a weakened stratospheric polar vortex (e.g., Polvani et al. 2017).

Similar to SAT, the JFM precipitation responses in the two subensembles of $\Delta past_{piSST}$ show striking differences, with opposite-signed meridional dipole patterns over the North Pacific and North Atlantic that result from the opposing circulation responses (Figs. 9a,b). The regression analysis reproduces many of the features of the subensembles over the North Atlantic and Arctic, but shows less agreement over the North Pacific (Figs. 9d,e). This is even more evident in the difference field: the regression analysis strongly underestimates the magnitude of the precipitation and SLP dipoles over the North Pacific, and the North Atlantic SLP trough extends farther to the east, which results in enhanced precipitation over the eastern North Atlantic and Iberian Peninsula, compared to the subensembles (Fig. 9f). These discrepancies highlight that

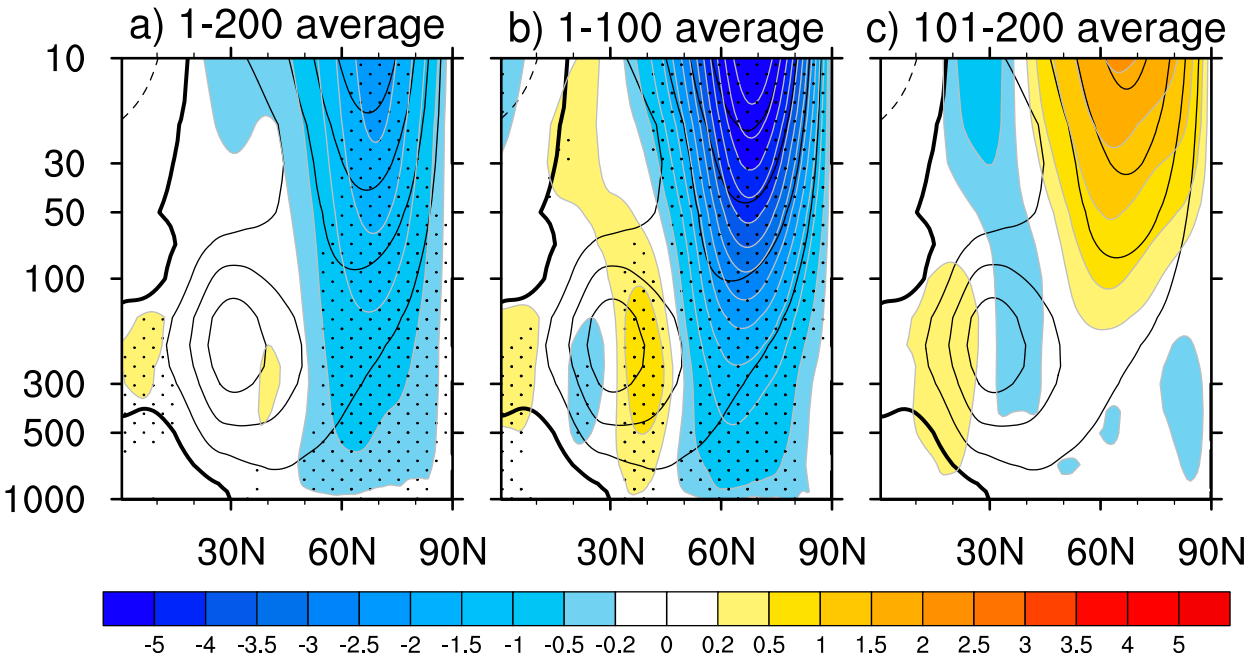

FIG. 4. DJF zonal-mean zonal wind response (shading; m s^{-1}) as a function of pressure (hPa; y axis) and latitude (x axis) for $\Delta\text{past}_{\text{piSST}}$ based on (a) all 200 members, (b) members 1–100, and (c) members 101–200. Black contours (interval of 10 m s^{-1}; zero contour is thickened) indicate the climatology. Stippling indicates the 90% statistical significance based on a two-sided Student's t test and false discovery rate (FDR; Wilks 2016).

while the stratosphere plays an important role, intrinsic variability of the tropospheric circulation also contributes to uncertainty in the simulated precipitation response to Arctic sea ice loss based on 100-member averages.

The influence of stratospheric internal variability on the tropospheric circulation and surface climate responses to Arctic sea ice loss is also apparent for the other sea ice loss cases, based on regression analysis of the bootstrapped samples of 100-member averages (Fig. 10; see also Figs. S4 and S5). Note that for these cases, the first and second 100-member averages do not necessarily mirror the Mean + 2σ and Mean − 2σ regression results, consistent with the chance sampling of U10 documented earlier (Figs. 3b–d). All cases, however, show a consistent NAM/NAO regression pattern with corresponding fingerprints in SAT and precipitation (Fig. 10c; see also Figs. S4 and S5). Likewise, the pattern and amplitude of the corresponding correlation results are also similar across the four cases. In particular, the correlation magnitudes reach ~0.6 for SAT in northeastern Siberia and Greenland and for precipitation in northern Europe and the Mediterranean region (Fig. S6). The consistency of the results across the four cases underscores the role of stratospheric internal variability in causing uncertainty in the surface climate response to Arctic sea ice loss when based on 100-member averages.

c. *Mechanism of stratospheric internal variability*

Previous studies have established a connection between the strength of the stratospheric polar vortex and upward planetary wave propagation from the troposphere (e.g., Polvani and Waugh 2004), indicating that stratospheric internal variability may originate, at least in part, in the troposphere. To investigate this possible dynamical linkage in $\Delta\text{past}_{\text{piSST}}$, we examine the monthly evolution of the zonal-mean eddy heat flux response near 100 hPa (model 0.1 hybrid sigma level) as a function of latitude in the two 100-member subensembles and the Mean + 2σ and Mean − 2σ regression results (Fig. 11). Consistent with the polar vortex response, the first 100-member average shows increased and statistically significant extratropical upward wave propagation in November–January (NDJ), while the second 100-member average shows insignificant and slightly decreased upward propagation in this season (Figs. 11a,b). Similar results are found in the regression analysis (Figs. 11d,e). Therefore, the different polar vortex responses between the first and second subensembles (recall Figs. 5a,b) is tied to internal variability of upward wave propagation. Similar results are found for the other sea ice loss cases (Fig. S7).

Changes in upward wave propagation have been found to be closely related to interactions between the anomalous and climatological planetary waves (in particular, zonal wavenumbers 1 and 2), which has been referred to as the linear wave interference theory (e.g., Garfinkel et al. 2010; Fletcher and Kushner 2011; Smith and Kushner 2012). This suggests that the different responses in upward wave propagation between the first and second 100 member averages of $\Delta\text{past}_{\text{piSST}}$ are also connected to constructive or destructive linear wave interference for zonal wavenumbers one and two. Indeed, the NDJ anomalous wave 1 is in phase with its climatology (constructive interference) poleward of 40°N in the first 100-member average, but no such relationship exists in the

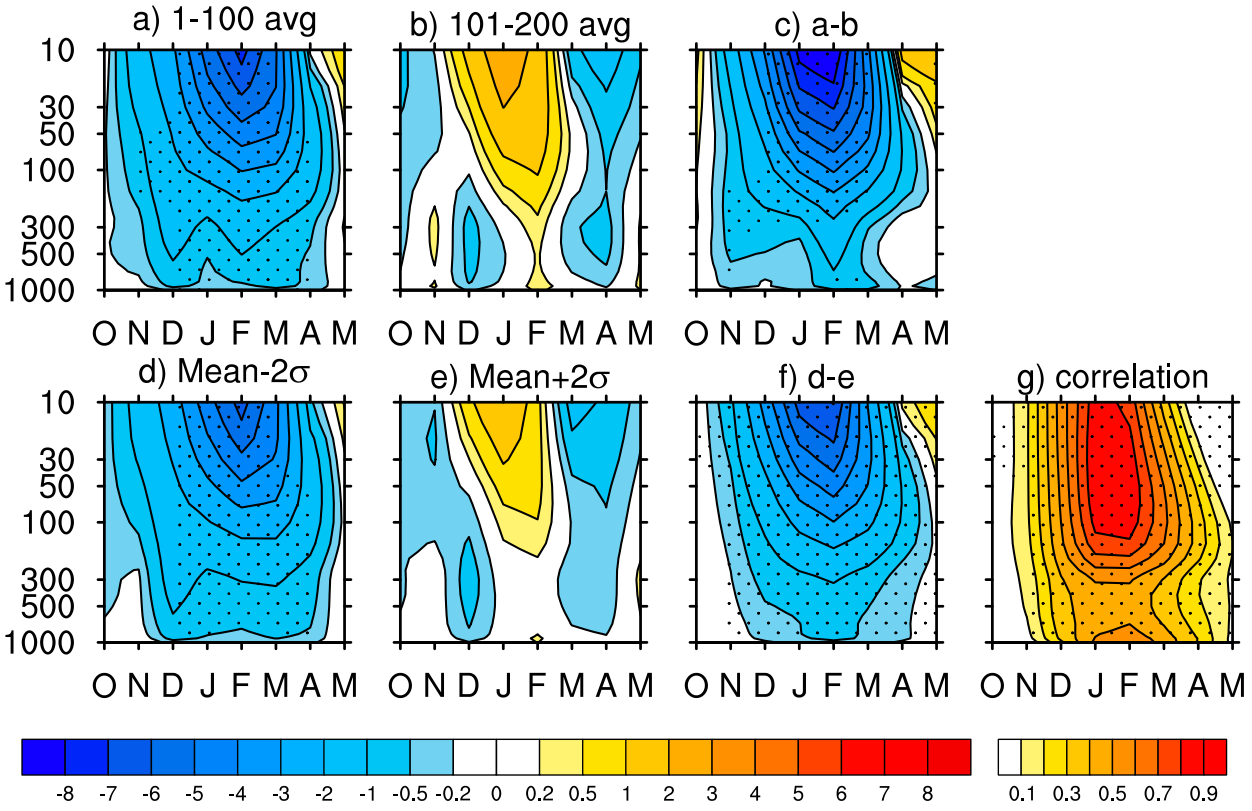

FIG. 5. (top) 60°N zonal-mean zonal wind response (m s^{-1}) in $\Delta past_{piSST}$ as a function of month (x axis) and pressure (y axis) for the (a) first 100-member average and (b) second 100-member average, and (c) their difference. (bottom) Regression analysis of 60°N zonal-mean zonal wind response onto U10 (defined as DJF zonal-mean zonal wind at 10 hPa and 60°N) across the 1000 bootstrapped samples of 100-member averages: (d) Mean $-$ 2σ, (e) Mean + 2σ, and (f) their difference. (g) Correlation of the zonal-mean zonal wind response with U10 across the 1000 bootstrapped samples. Stippling indicates the 90% statistical significance based on a two-sided Student's t test and false discovery rate.

second 100-member average (Figs. 12a,b). Similarly, while anomalous wave 2 is in quadrature with the climatology in the first 100-member average, it is out of phase with the climatology (destructive interference) in the second 100-member average (Figs. 12a,b). As a result, there will be more wave-1 and wave-2 upward wave propagation in the first 100-member average than the second. The regression analysis shows similar results regarding wave-1 and wave-2 interference characteristics (Figs. 12d,e), confirming that internally driven planetary wave interference can largely explain the different upward wave propagation and polar vortex responses in 100-member averages. Similar features can be also seen in the other sea ice loss cases (Figs. S8 and S9), suggesting that this is a universal mechanism connecting internal variability of the stratosphere and troposphere.

d. *Role of the ensemble size in stratospheric internal variability*

While the preceding analysis has focused on 100-member averages, we next investigate the role of ensemble size in determining the magnitude of stratospheric internal variability and its impact on the assessment of the tropospheric response to sea ice loss. To do this, we calculate the 2.5th–97.5th-percentile (-2σ to $+2\sigma$) range of U10 as a function of sample size (number of ensemble members averaged) using the analytical formula in Eq. (5) for both model and reanalysis. The U10 interannual σ in pdSST-pdSIC (assuming it is equivalent to the standard deviation across 200 ensemble members) is 10.0 m s^{-1} (similar values obtain in the other PAMIP experiments), which is very close to the value of 9.6 m s^{-1} found in the National Centers for Environmental Prediction (NCEP)–NCAR reanalysis (Kalnay et al. 1996) based on detrended data during 1966–2020 when the data are most reliable (see Fig. S10). Thus, the curves showing the 2.5th–97.5th-percentile ranges of U10 response as a function of ensemble size are nearly identical for CAM6 and the NCEP–NCAR reanalysis data (herein simply "Reanalysis"; Fig. 13a). This means that the signal-to-noise ratios of the U10 responses in each of the four sea ice loss cases would be similar if the "observed" noise were substituted for the model's noise. In particular, we note that the 2σ uncertainty based on 200-member averages (2.0 m s^{-1} for CAM6 and 1.9 m s^{-1} for Reanalysis; Fig. 13a) exceeds the magnitude of the 200-member averaged U10 response for each of the 4 ice loss cases (-1.6, -0.7, -0.4, and 0.5 m s^{-1} for $\Delta past_{piSST}$, $\Delta past_{pdSST}$, Δfut_{pdSST}, and Δfut_{futSST}, respectively). Thus, our conclusions

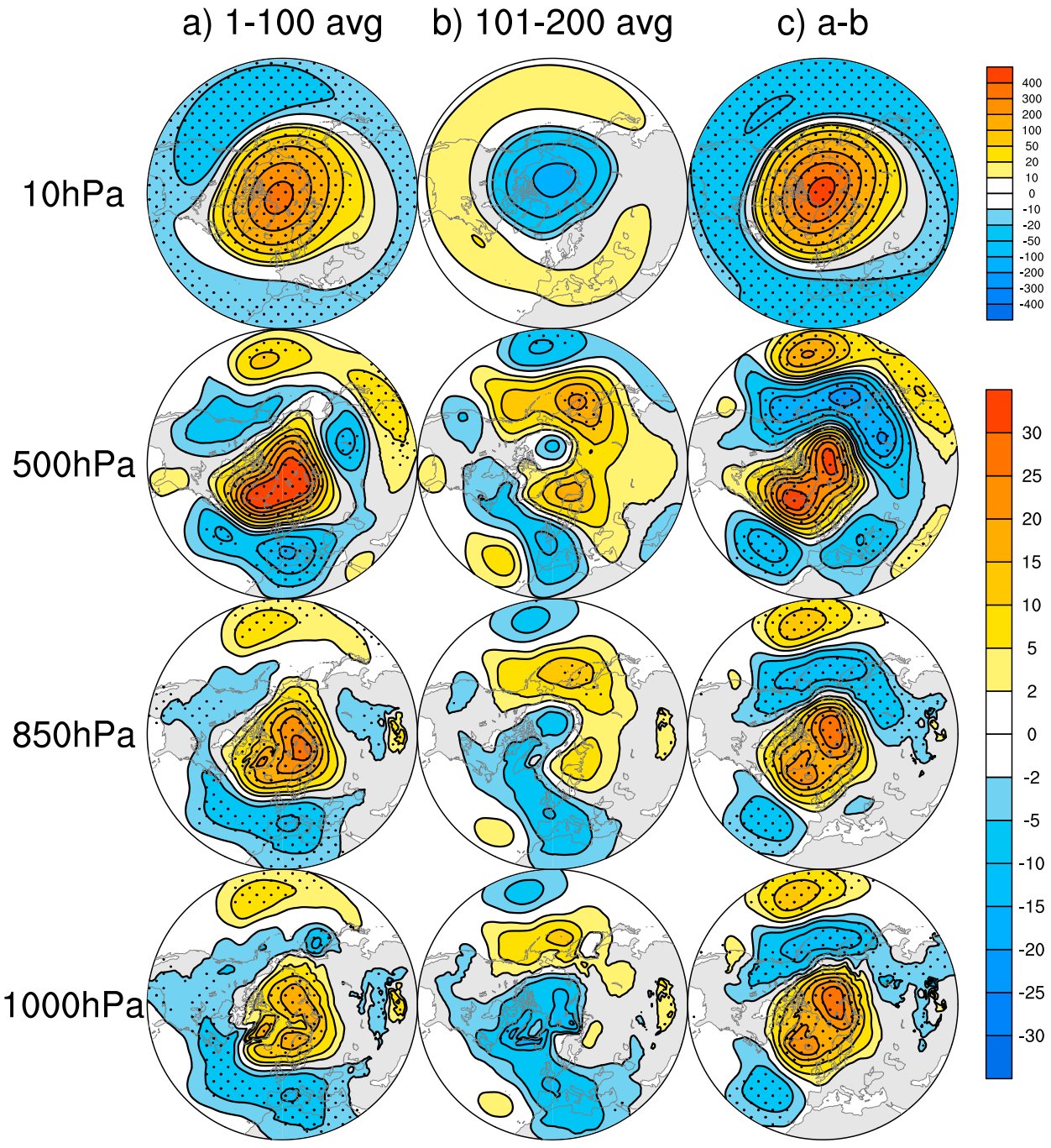

FIG. 6. Geopotential height response (m) in $\Delta\text{past}_{\text{piSST}}$ for the (a) first 100-member average and (b) second 100-member average, and (c) their difference. (from top to bottom) The 10-hPa DJF response and the 500-, 850- and 1000-hPa responses in JFM, respectively. Stippling indicates the 90% statistical significance based on a two-sided Student's *t* test and false discovery rate.

regarding the effect of stratospheric internal variability on the signal-to-noise of the U10 response to ice loss remain valid if using "observed" noise. It should be noted that our estimate of interannual U10 σ reflects internal atmospheric variability only in CAM6, whereas in Reanalysis coupled ocean–atmosphere and land–atmosphere interactions may also contribute. However, in this regard, we note that the interannual U10 σ in a long preindustrial control simulation of CAM6 is only 2% smaller than that of the fully coupled Community Earth System Model version 2 (CESM2).

Next, we assess the impact of internal U10 variability on the response of the NAO (normalized PC1 of SLP in the Atlantic–European sector) as a function of sample size based on CAM6 and Reanalysis data. As before, we compute the

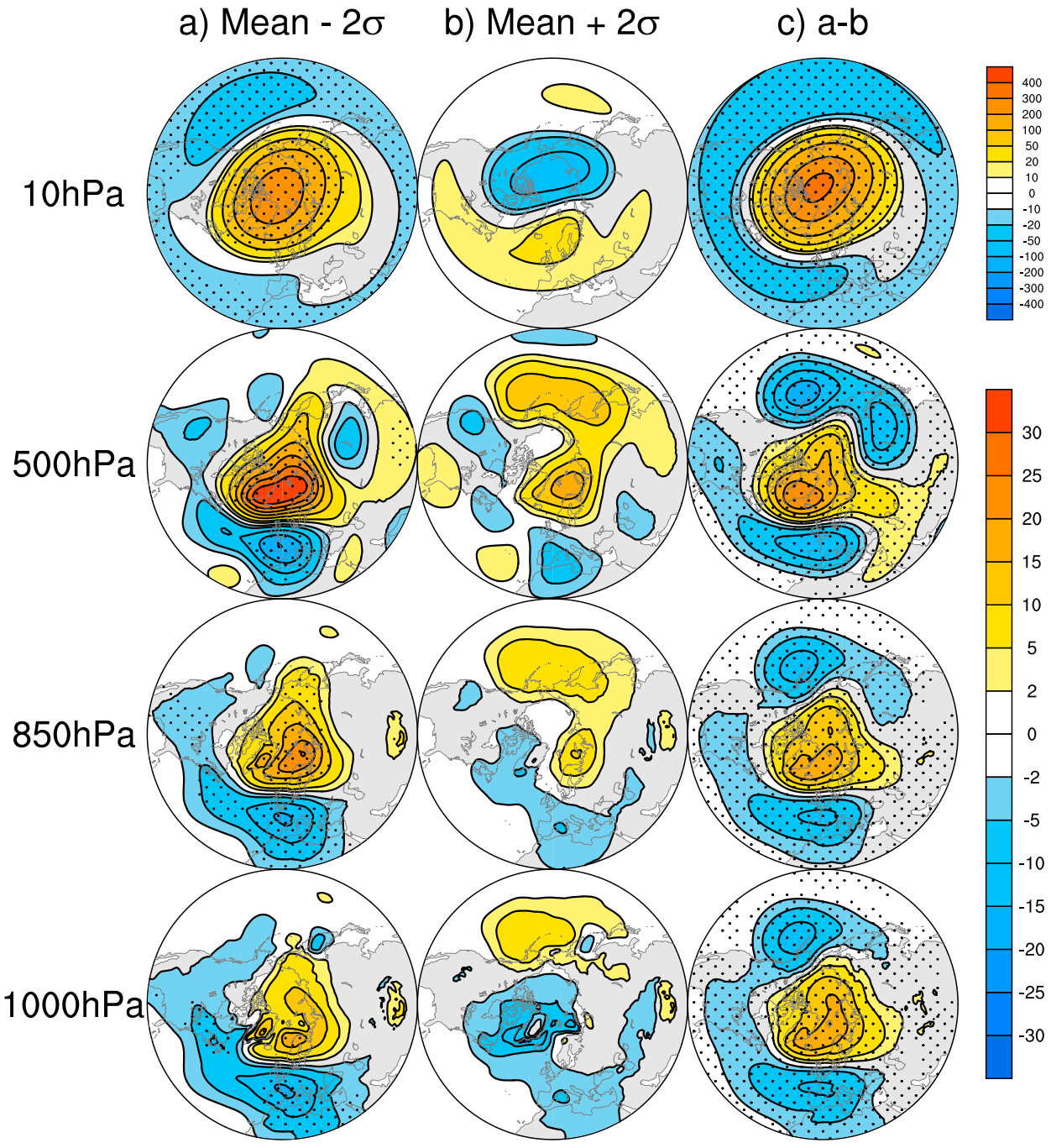

FIG. 7. Regression analysis of geopotential height response onto U10 in $\Delta\text{past}_{\text{piSST}}$ across the 1000 bootstrapped samples: (a) Mean − 2σ, (b) Mean + 2σ, and (c) their difference. (from top to bottom) The 10-hPa DJF response and the 500-, 850- and 1000-hPa responses in JFM, respectively. Stippling indicates the 90% statistical significance based on a two-sided Student's *t* test and false discovery rate.

regression coefficient of the normalized JFM NAO index onto the normalized DJF U10 index based on interannual anomalies (detrended in the case of Reanalysis) and use this value in Eq. (5) (section 2d). For a sample size of one, the proportion of internal NAO variability associated with U10 is slightly smaller for reanalysis data (1.4) than for the model (1.8), and the difference (scaled by $1/\sqrt{N}$) is maintained for all sample sizes (Fig. 13b). This indicates that either the model overestimates the linkage between the stratospheric polar vortex and the surface NAO, or such linkage is represented correctly in the model but there is just more, unrelated variability in the observations. For the case of a 200-member average, the minimum ensemble size needed for the JFM NAO response in CAM6 to be significantly different from

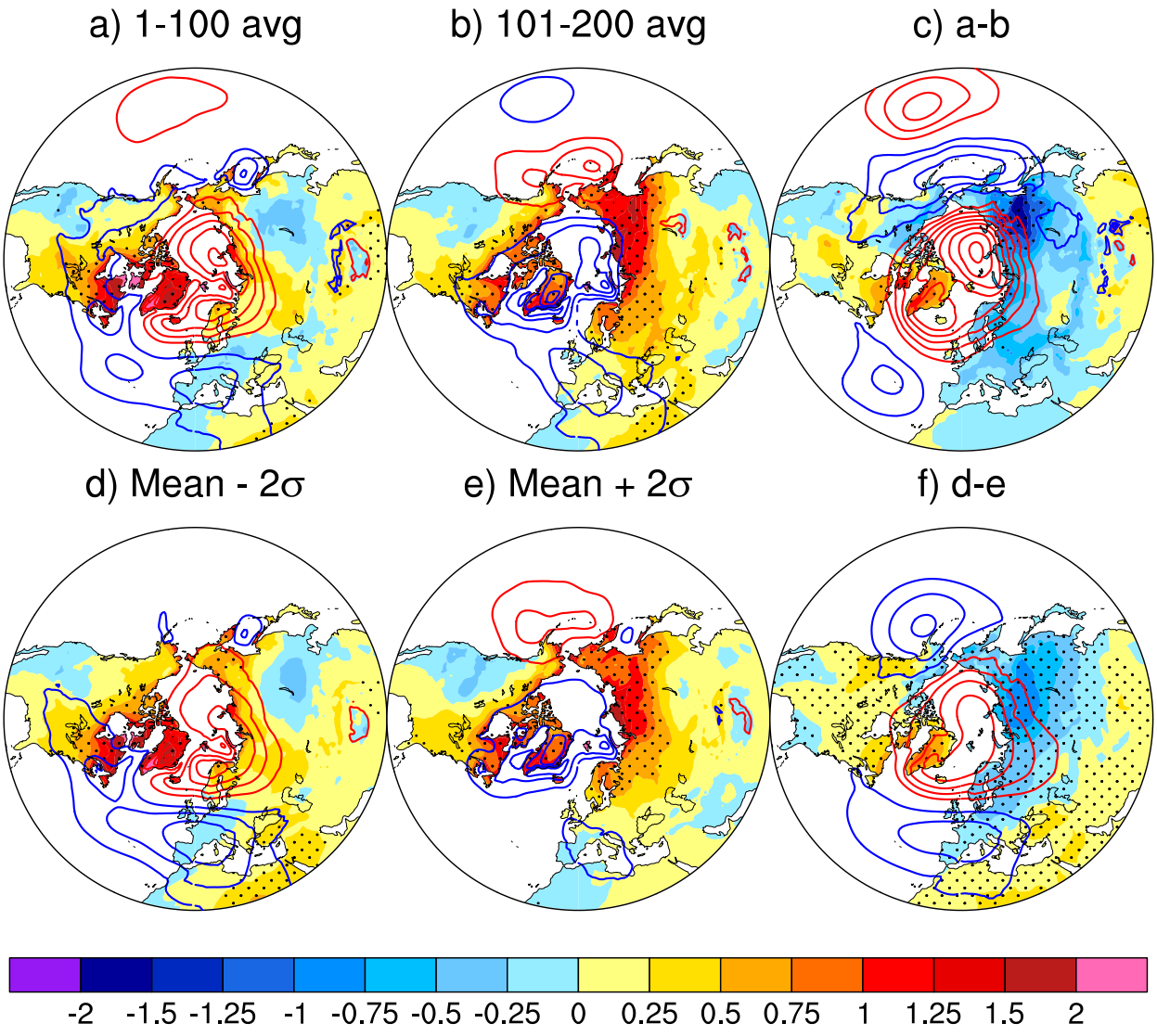

FIG. 8. (top) JFM SAT (shading; °C) and SLP (contours; interval of 0.5 hPa) responses in $\Delta\text{past}_{\text{piSST}}$ for the (a) first 100-member average and (b) second 100-member average, and (c) their difference. (bottom) Regression analysis of JFM SAT response onto U10 in $\Delta\text{past}_{\text{piSST}}$ across the 1000 bootstrapped samples of 100-member averages: (d) Mean $-$ 2σ, (e) Mean + 2σ, and (f) their difference. Red and blue contours denote positive and negative values, respectively. Zero contour line has been omitted. Stippling indicates the 90% statistical significance based on a two-sided Student's *t* test and false discovery rate.

zero at the 95% confidence level is 165, 1296, 144, and 73 for $\Delta\text{past}_{\text{piSST}}$, $\Delta\text{past}_{\text{pdSST}}$, $\Delta\text{fut}_{\text{pdSST}}$, and $\Delta\text{fut}_{\text{futSST}}$, respectively, due to the high level of stratospherically induced noise in the NAO.

4. Implications for attributing observed trends to Arctic sea ice loss

Motivated by empirical observational studies examining the relationship between trends in atmospheric circulation and Arctic warming (or sea ice loss) with inferences about causality (e.g., Francis and Vavrus 2012), we proceed to apply our CAM6 results to the interpretation of observed trends in recent decades. We first note that the "past" sea ice loss adopted for the PAMIP protocol is approximately equivalent to the observed [merged Hadley–Optimum Interpolation (OI) sea ice concentration; Hurrell et al. (2008)] linear change during 1971–2020 for the November–March average (almost identical ice area loss with similar spatial distribution; Fig. S11). Using the analytical approach of Thompson et al. (2015) and Deser et al. (2017), we calculate the 95% margin of error (e) on a 50-yr linear trend from the statistics of the interannual σ and 1-yr lag autocorrelation (r_1) for a Gaussian time series as follows. Equation (6) shows the dependence of e on σ and r_1:

$$e = t_c n_t \sigma_{\text{sfc}} \gamma(n_t, r_1) g(n_t), \tag{6}$$

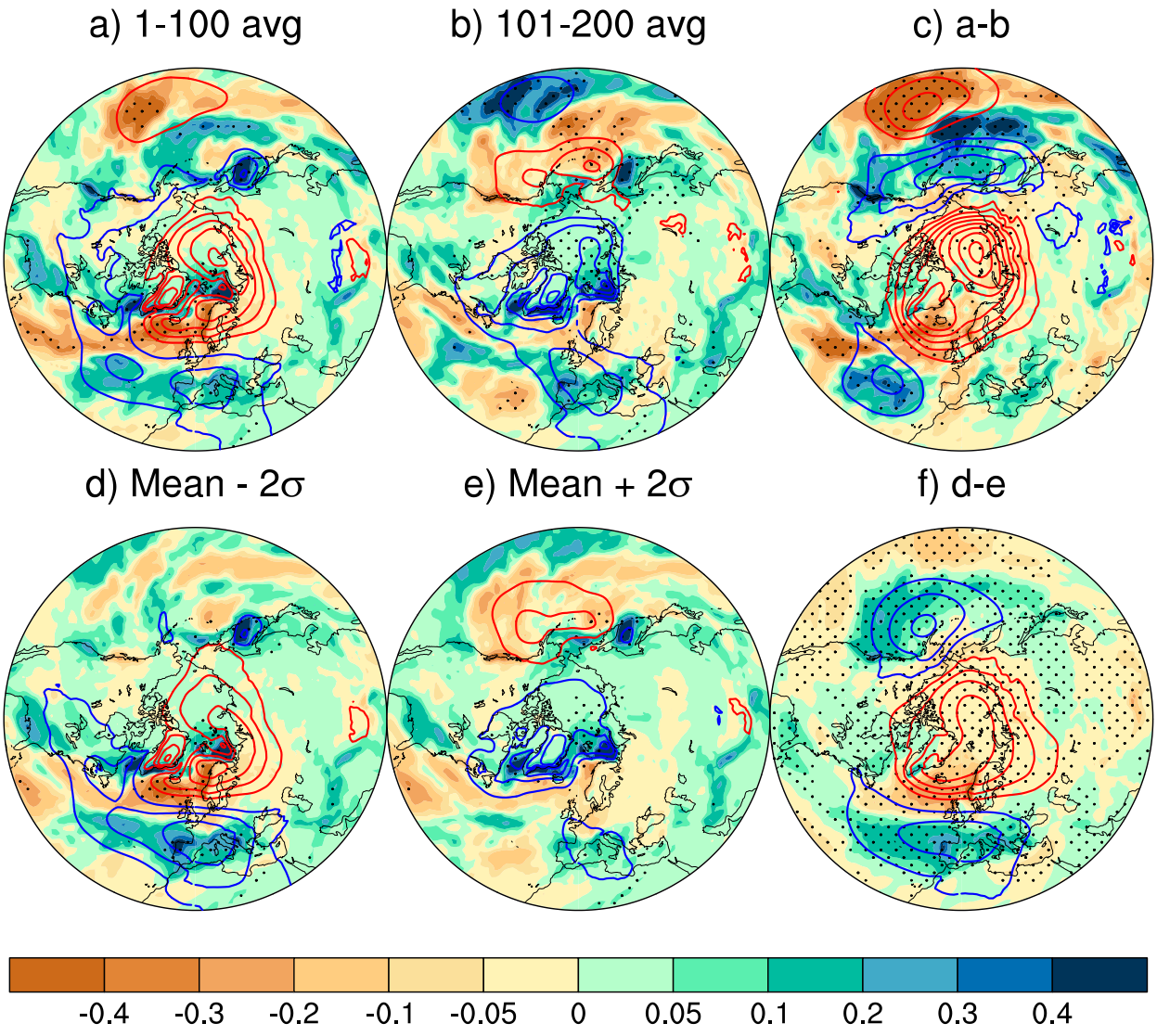

FIG. 9. (top) JFM precipitation (shading; mm day^{-1}) and SLP (contours; interval of 0.5 hPa) responses in $\Delta\text{past}_{\text{piSST}}$ for the (a) first 100-member average and (b) second 100-member average, and (c) their difference. (bottom) Regression analysis of JFM precipitation response onto U10 in $\Delta\text{past}_{\text{piSST}}$ across the 1000 bootstrapped samples of 100-member averages: (d) Mean $-$ 2σ, (e) Mean $+$ 2σ, and (f) their difference. Red and blue contours denote positive and negative values, respectively. Zero contour line has been omitted. Stippling indicates the 90% statistical significance based on a two-sided Student's t test and false discovery rate.

where $t_c = 2$ (95% confidence level), n_t is the length of the trend in years (50), σ_{sfc} is the value of the surface anomaly (SLP, SAT or precipitation) associated with a one σ anomaly of U10, and the other terms are defined as follows:

$$\gamma(n_t, r_1) = \left[\frac{n_t - 2}{n_t\left(\frac{1 - r_1}{1 + r_1}\right) - 2}\right]^{1/2}, \tag{7}$$

$$g(n_t) = \sqrt{\frac{12}{n_t^3 - n_t}}. \tag{8}$$

Figure 14 shows maps of the 95% margin of error on a 50-yr trend in SLP (top row), SAT (middle row), and precipitation (bottom row) associated with internal variability of the stratospheric polar vortex (U10) based on Reanalysis (first column) and CAM6 (middle column) following the procedure outlined above. Overall, CAM6 shows a realistic depiction of the patterns and magnitudes seen in Reanalysis, including the NAO and its fingerprint on SAT and precipitation. There are some notable differences as well. For example, the observed SLP pattern more closely resembles the regional NAO while the model's pattern is more similar to the hemispheric NAM. As a result, the precipitation values over the North Pacific differ between Reanalysis and CAM6. These discrepancies may be related to the additional influence of El Niño–Southern Oscillation (ENSO) on U10 variability in Reanalysis that is lacking in CAM6 due to the use of

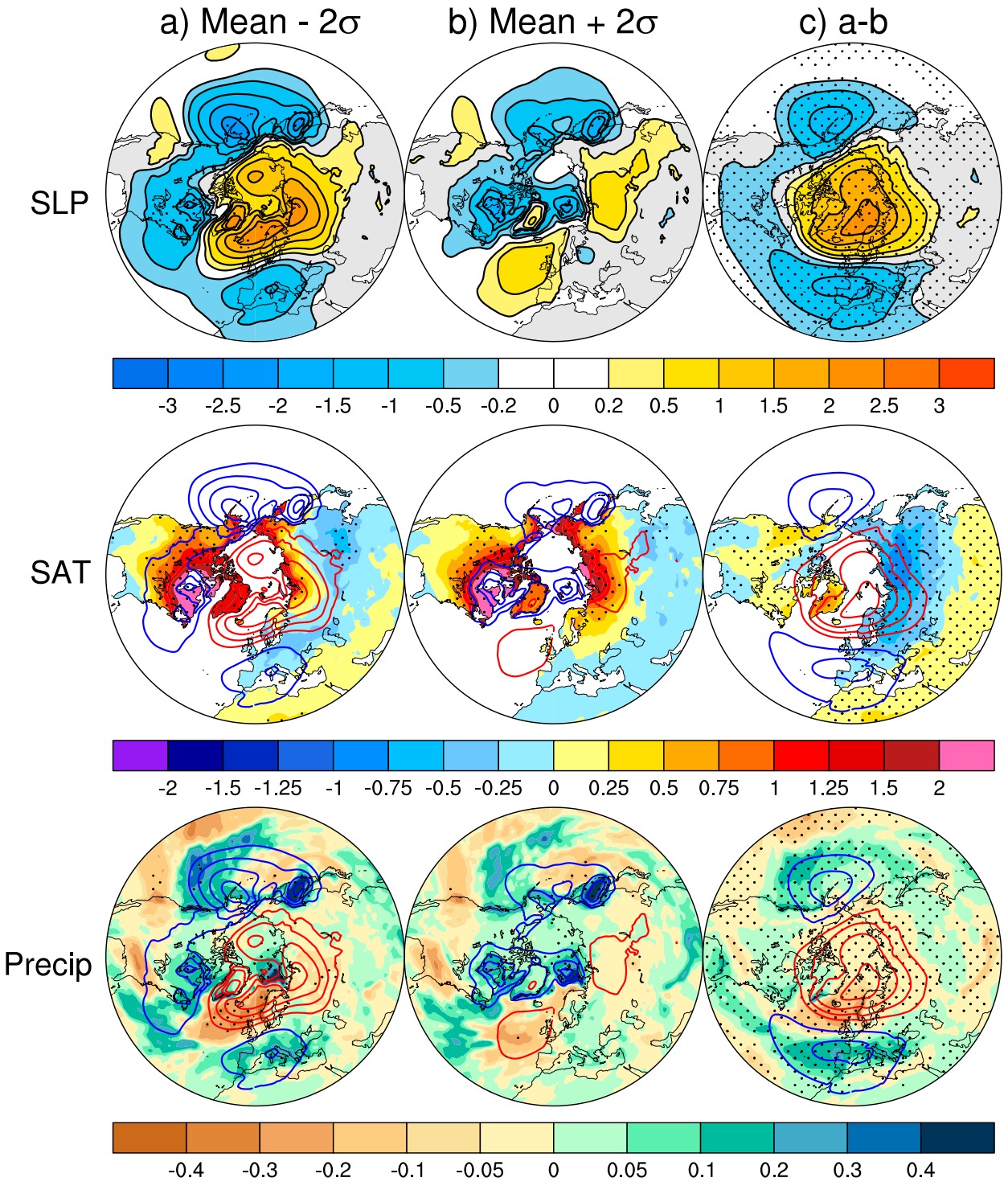

FIG. 10. Regression analysis of JFM response onto U10 in Δfut_{pdSST} across the 1000 bootstrapped samples of 100-member averages. (from top to bottom) The SLP (shading; hPa), SAT (shading; °C), and precipitation (shading; mm day^{-1}) responses, respectively. (a) Mean − 2σ, (b) Mean + 2σ, and (c) their difference. The SLP responses (contours; interval of 0.5 hPa) are overlaid on the SAT and precipitation panels. Red and blue contours denote positive and negative values, respectively. Zero contour line has been omitted. Stippling indicates the 90% statistical significance based on a two-sided Student's *t* test and false discovery rate.

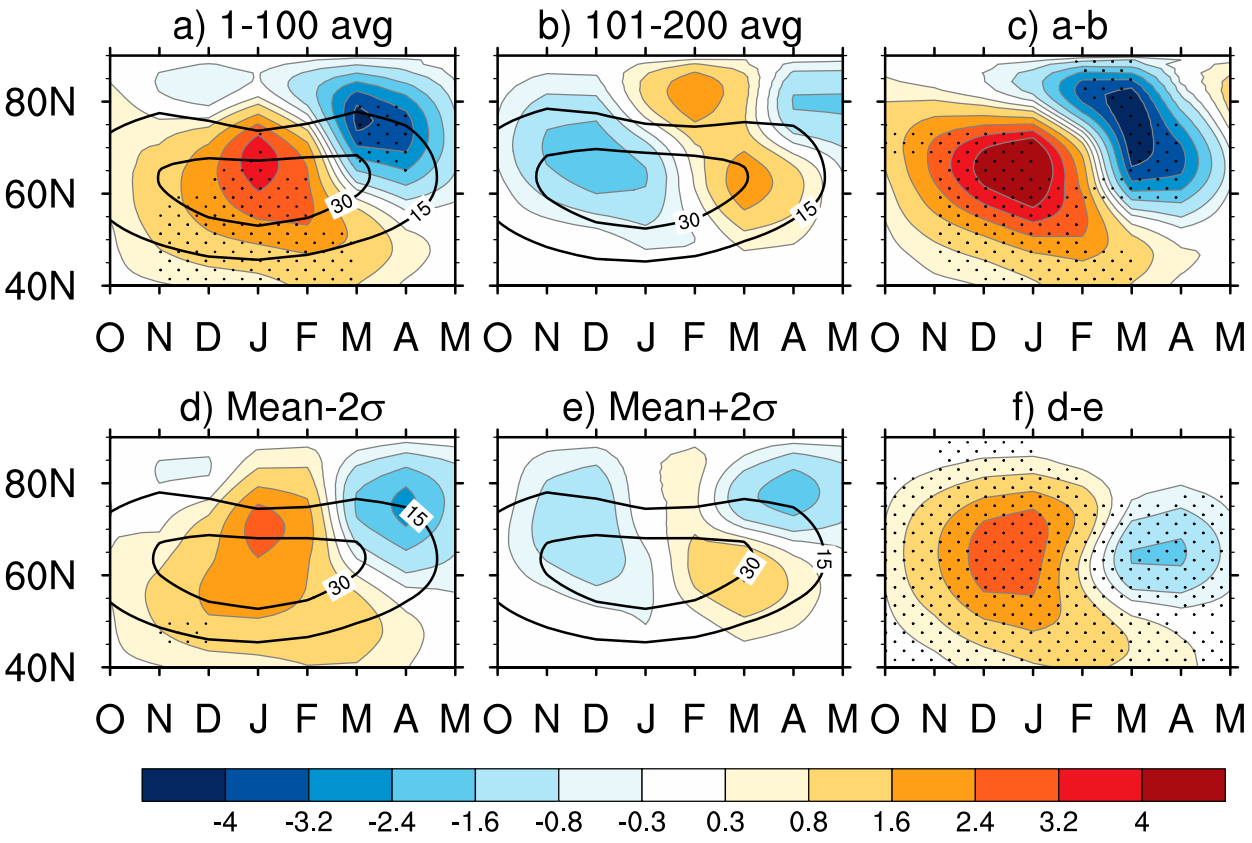

FIG. 11. (top) Eddy heat flux response near 100 hPa (model hybrid 0.1 sigma level; shading; K m s^{-1}) in $\Delta past_{piSST}$ as a function of month (x axis) and latitude (y axis) for the (a) first 100-member average and (b) second 100-member average, and (c) their difference. (bottom) Regression analysis of eddy heat flux response near 100 hPa onto U10 across the 1000 bootstrapped samples of 100-member averages: (d) Mean $-$ 2σ, (e) Mean + 2σ, and (f) their difference. Stippling indicates the 90% statistical significance based on a two-sided Student's t test and false discovery rate. The climatologies (contours; interval of 15 K m s^{-1}) are overlaid on (a), (b), (d) and (e).

a climatological seasonal cycle as the SST boundary condition, or it may be a reflection of the well-known bias of atmospheric models to simulate a more zonally symmetric NAM structure of variability compared to the more regionally confined NAO structure found in observations (Flato et al. 2013). Over the North Atlantic midlatitudes, the SLP trough is shifted eastward in CAM6 compared to Reanalysis, with impacts on precipitation over the Mediterranean region. This bias appears to be a common issue in climate models (e.g., Sigmond et al. 2013; Ayarzagüena et al. 2020).

Despite some regional differences in magnitude and pattern, the margin of error on the surface climate trends associated with U10 in both CAM6 and Reanalysis substantially exceed the magnitude of the CAM6 response to the observed Arctic sea ice loss trend during 1971–2020, obtained by combining the 200-member averages of $\Delta past_{piSST}$ and $\Delta past_{pdSST}$ (see above; Fig. 14c). Therefore, unless the model's forced response is substantially underestimated (as some studies suggest: e.g., Mori et al. 2019a) or the model substantially overestimates stratospheric internal variability [e.g., the signal-to-noise paradox documented in Smith et al. (2020)], it will be difficult to isolate the forced surface climate response to recent Arctic sea ice loss from stratospherically induced internal variability in observations.

5. Summary and discussion

a. Summary

In this study, we conduct PAMIP time-slice experiments with CAM6 to investigate the atmospheric response to past and projected Arctic sea ice loss, with a specific focus on the role of stratospheric internal variability on the uncertainty in the tropospheric circulation and surface climate response based on 100-member ensembles. Our focus on 100-member averages is motivated by the PAMIP protocol recommendation. We note that increasing the sample size N will reduce the regression magnitudes by a factor of $1/\sqrt{N}$ (Fig. 5f and Fig. S12c), but will not affect the correlation magnitudes. Our main findings are summarized as follows.

1) Consistent with previous studies, the seasonal cycle of the Arctic and terrestrial high-latitude SAT and precipitation responses is approximately in phase with that of the Arctic surface energy flux response, which maximizes in winter (October–March), rather than that of the ice loss, which

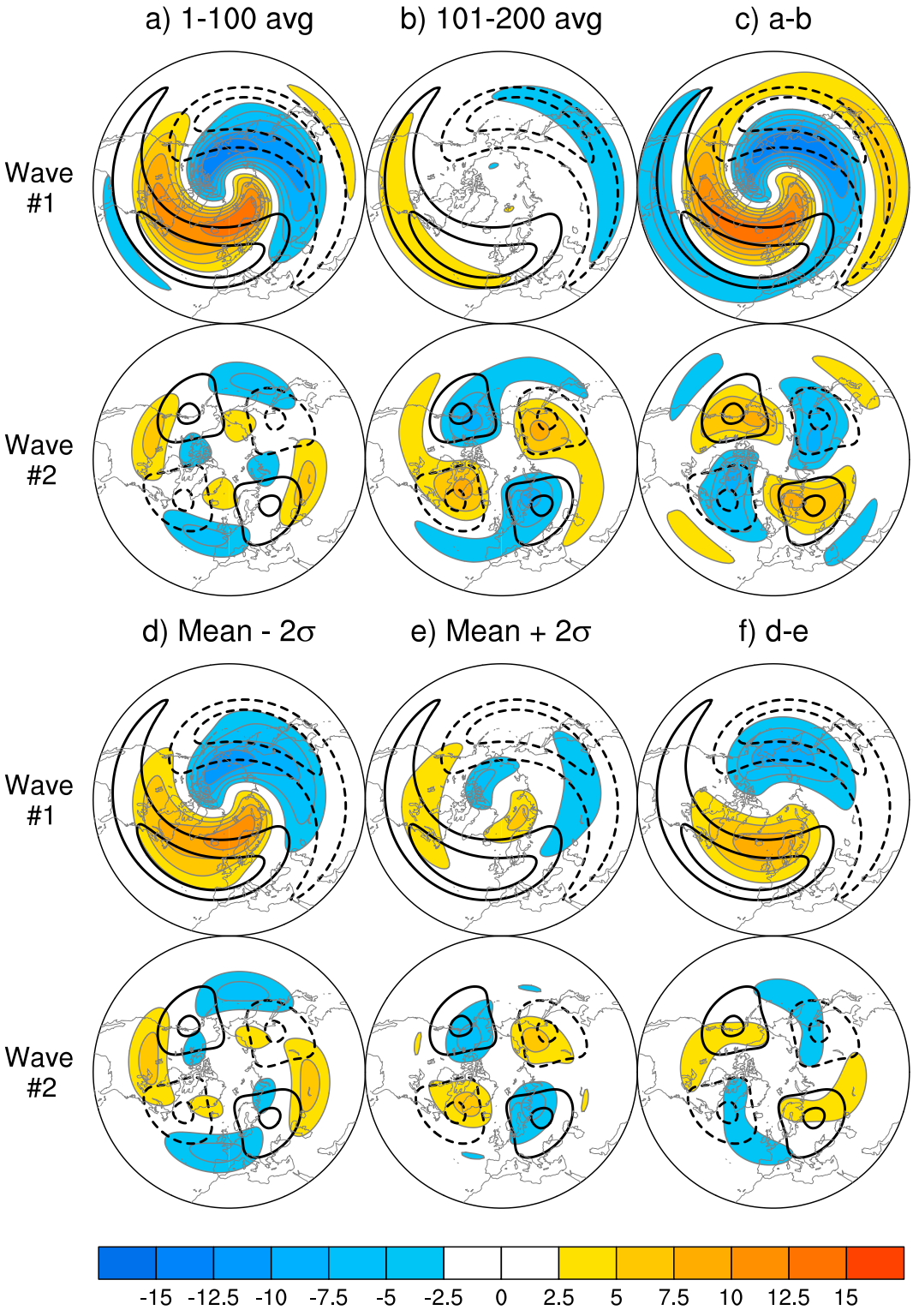

FIG. 12. (top two rows) NDJ zonal wave-1 and wave-2 responses (shading; m) at 300 hPa in $\Delta\text{past}_{\text{piSST}}$ for the (a) first 100-member average and (b) second 100-member average, and (c) their difference. The climatologies (contours; interval of 50 m) are overlaid in (a)–(c). (bottom two rows) Regression analysis of NDJ zonal wave-1 and wave-2 responses at 300 hPa onto U10 in $\Delta\text{past}_{\text{piSST}}$ across the 1000 bootstrapped samples of 100-member averages: (d) Mean $-$ 2σ, (e) Mean + 2σ, and (f) their difference. The climatologies (contours; interval of 50 m) are overlaid in (d)–(f). Solid and dashed contours denote positive and negative values, respectively. The zero contour line has been omitted.

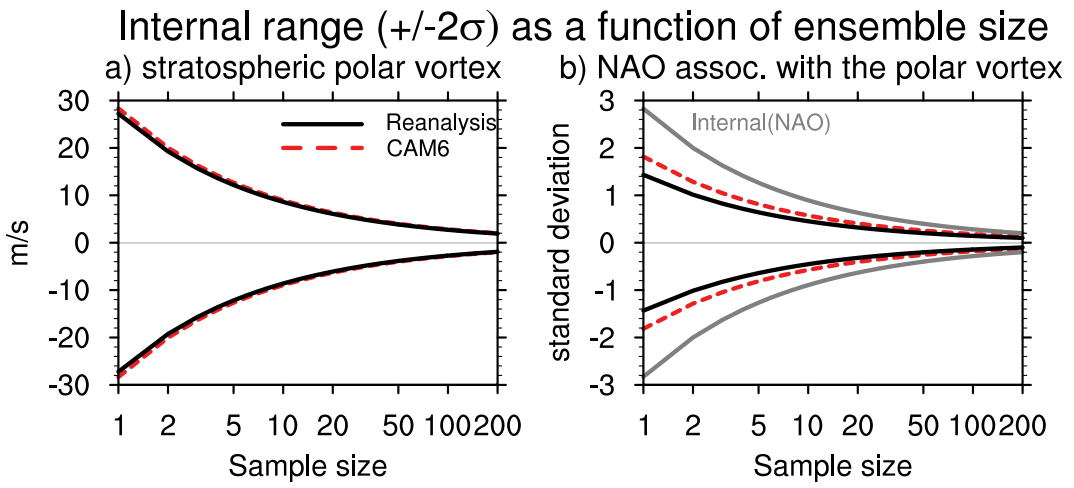

FIG. 13. (a) 2.5th–97.5th-percentile (2σ) range of variability in DJF U10 (m s^{-1}) as a function of the number of ensemble members averaged ("sample size") in Reanalysis data (red curve) and CAM6 (black curve). (b) As in (a), but for the JFM NAO response associated with the plus and minus two standard deviation anomaly of DJF U10. Gray curve indicates the total NAO internal variability ($\pm 2\sigma$) in Reanalysis and CAM6 (identical because each NAO time series is standardized by its interannual standard deviation).

peaks in autumn (September–October). The internal variability in Arctic surface energy flux response based on 100-member averages is small.

2) Unlike the surface responses, the magnitude of the winter stratospheric polar vortex response to both past and future Arctic sea ice loss is small compared to its internal variability, even when based on 100-member averages. The stratospheric internal variability is associated with large uncertainty in the tropospheric circulation response to sea ice loss, and can completely obscure the forced NAM/NAO circulation response and associated impacts on air temperatures over Eurasia and eastern North America and precipitation over the North Atlantic and Mediterranean Sea based on 100-member averages.
3) Internal variability of the winter stratospheric polar vortex is related to antecedent conditions in tropospheric wave activity. As such, it can be explained by internal variability in upward wave propagation and linear wave interference theory.
4) CAM6 exhibits realistic magnitudes of interannual variability in the winter stratospheric polar vortex and its connection to the surface NAO when compared against detrended Reanalysis data during 1966–2020. If the interannual variability of the stratospheric polar vortex is mainly due to internal atmospheric dynamics (including coupling with the troposphere), then Reanalysis data can be used to assess the uncertainty of the atmospheric circulation response to Arctic sea ice loss based on 100-member averages following the analytical approach developed by Thompson et al. (2015). The resulting signal-to-noise for the winter (JFM) SLP response to past Arctic sea ice loss is low (<1) based on 100-member (or 200-member) averages, indicating that unless the model's forced response is substantially underestimated or the model substantially overestimates stratospheric internal variability, it will be difficult to isolate the forced response to recent Arctic sea ice loss in nature.

b. Discussion

The results presented above highlight a number of issues. The first one concerns the observed relationship between Arctic sea ice and winter NAO/NAM (e.g., Cohen 2016), which has been hypothesized to reflect a causal influence of Arctic sea ice loss via a stratospheric pathway (Ruggieri et al. 2016) and argued to be one of the dominant climate impacts in recent years (Jaiser et al. 2016). In agreement with Barnes and Screen (2015) and P21, but based on an explicit consideration of the stratospheric pathway, our results caution that empirical analyses that rely on only four decades of observations may face serious sampling issues. Indeed, while Arctic sea ice extent has declined more or less continuously since 1979, the stratospheric polar vortex does not show any significant trend over this time period, but instead exhibits mainly interannual to decadal variability (Fig. S10). Moreover, the observed connection between Arctic sea ice and NAM/NAO has weakened when more recent data (e.g., years 2013–20) are included in the analysis (Smith et al. 2022), suggesting that part of the relationship may result from stratospheric internal variability and its downward influence on the troposphere.

The second issue regards the relative roles of stratospheric versus tropospheric pathways for the forced response to Arctic sea ice loss. When averaged over all 200 members, the polar vortex response shows large variation across the four sea ice loss cases (from −1.6 to 0.5 m s^{-1}; Fig. 3), while the tropospheric circulation responses are quite similar (not shown). Thus, in CAM6, the atmospheric circulation change due to Arctic sea ice loss is mainly dominated by the tropospheric pathway, with a relatively smaller role for the stratospheric pathway. Interestingly, a recent PAMIP multimodel

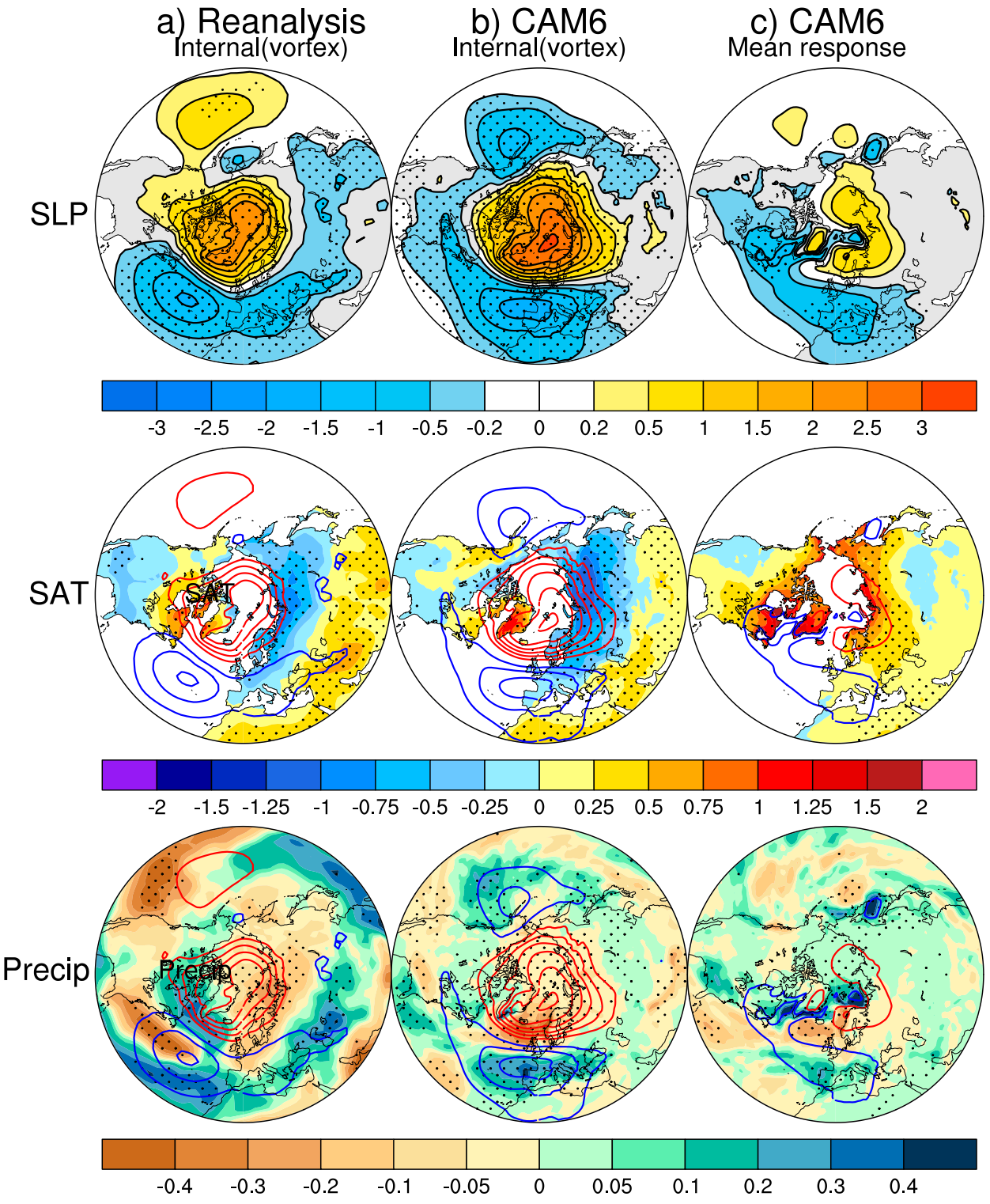

FIG. 14. (a) 95% marginal error (2σ) of the JFM linear trend during the past 50 years (1971–2020) for (from top to bottom) SLP (shading; hPa), SAT (shading; °C), and precipitation (shading; mm day^{-1}) based on (a) NCEP–NCAR reanalysis data and (b) CAM6 (see text for details). The SLP trends are overlaid as contours (interval of 0.5 hPa) on the SAT and precipitation panels. (c) The estimated forced response to Arctic sea ice loss over the past 50 years from the CAM6 experiments (see text for details). Stippling indicates the 90% statistical significance based on a two-sided Student's t test and false discovery rate.

analysis also found divergent stratospheric polar vortex responses but robust tropospheric responses (Smith et al. 2022). Note that these findings do not negate the importance of considering sampling variability in the stratospheric polar vortex response and its impact on the troposphere.

The third issue concerns the relative roles of internal variability in the stratosphere versus troposphere. P21 found that the tropospheric circulation, either due to intrinsic atmospheric dynamics or ENSO-related teleconnections, is the main source of internal variability in their PAMIP experiments with SC-WACCM4, while we find that internal variability of the stratospheric polar vortex plays a dominant role in our CAM6 experiments. These results do not contradict each other and can be easily reconciled. As shown in Fig. 3, the polar vortex response difference between the first and second 100 members can be large or small solely by chance. When the two 100-member averages show similar U10 responses, like in the $\Delta past_{pdSST}$ and Δfut_{futSST} sea ice loss cases, the contribution of internal variability unrelated to the stratosphere will manifest itself in a manner similar to that in P21 (not shown). On the other hand, when the two 100 member-averages of U10 show large differences, as in $\Delta past_{piSST}$ and Δfut_{pdSST}, the difference in the tropospheric responses will manifest primarily as an NAO/NAM pattern induced by stratospheric internal variability. More importantly, we have shown that a random selection of 100 members of any of the CAM6 PAMIP sea ice loss experiments is likely to contain substantial stratospheric internal variability, with consequences for the signal-to-noise ratio of the tropospheric and surface climate responses. We note that our results are in agreement with newer PAMIP modeling studies, such as that of Streffing et al. (2021), who used the Open Integrated Forecasting System, albeit with a focus on the sensitivity to horizontal resolution as opposed to stratospheric internal variability per se. It is also worth mentioning that stratospheric internal variability is not the only source of uncertainty in the tropospheric response to Arctic sea ice loss, but it is substantial (Fig. S13; also inferred from Fig. S6).

The fourth issue concerns the mechanisms of stratospheric internal variability. In addition to the eddy heat flux diagnostics (Fig. 11), we also examined the November–January wave activity flux (Plumb 1985) and find very different upward wave propagation responses over Siberia between the two 100-member subensembles, underscoring the important role of tropospheric internal variability in modulating upward wave propagation characteristics through interference with the climatological planetary waves (not shown). Further research is needed to assess additional mechanisms such as troposphere–stratosphere resonance of free modes (Tung and Lindzen 1979; Plumb 1981; Esler and Scott 2005) and interactions between the polar vortex and Aleutian anticyclone (O'Neill and Pope 1988; Scott and Dritschel 2006).

Our results come with several caveats. CAM6 is a "low-top" model, and as such it does not internally generate a QBO and thus lacks mechanisms that may be sensitive to the phase of the QBO (e.g., Labe et al. 2019). Although the magnitude of its stratospheric internal variability is realistic (Figs. 13 and 14), the mean winter polar vortex is too strong, causing the simulated frequency of sudden stratospheric warmings to be underestimated (Ayarzagüena et al. 2020). It is still unclear whether the stratospheric response to Arctic sea ice loss may depend on the basic state bias in the polar vortex (e.g., Sigmond and Scinocca 2010; Sun et al. 2015). Finally, our atmosphere-only model experiments do not consider the role of ocean–atmosphere coupling, which has been shown to amplify the response to Arctic sea ice loss (Deser et al. 2016) and expand its reach to the entire globe (e.g., Deser et al. 2015; Tomas et al. 2016; Wang et al. 2018; P21).

Last but not least, it is still an open question whether models underestimate the atmospheric response to Arctic sea ice loss (e.g., Mori et al. 2019a) and associated signal-to-noise ratio (e.g., Smith et al. 2020). So far there is still no consensus (e.g., Screen and Blackport 2019; Mori et al. 2019b), but nonstationarity of the connection between sea ice reduction and atmospheric circulation (Kolstad and Screen 2019; Blackport and Screen 2020) appears to imply large internal variability in observations. In other words, the connection may be an artifact of sampling.

Acknowledgments. We appreciate the thoughtful comments and suggestions of three anonymous reviewers, and constructive discussions with Dr. Walter A. Robinson (NCSU). NCAR is sponsored by the National Science Foundation. We would like to acknowledge the use of computational resources (https://doi.org/10.5065/D6RX99HX) at the NCAR–Wyoming Supercomputing Center provided by the National Science Foundation and the State of Wyoming, and supported by NCAR's Computational and Information Systems Laboratory.

Data availability statement. The PAMIP data with CAM6 are accessible on the Earth System Grid Federation website (https://doi.org/10.22033/ESGF/CMIP6.2197).

REFERENCES

Audette, A., and Coauthors, 2021: Opposite responses of the dry and moist eddy heat transport into the Arctic in the PAMIP experiments. *Geophys. Res. Lett.*, **48**, e2020GL089990, https://doi.org/10.1029/2020GL089990.

Ayarzagüena, B., and Coauthors, 2020: Uncertainty in the response of sudden stratospheric warmings and stratosphere–troposphere coupling to quadrupled CO_2 concentrations in CMIP6 models. *J. Geophys. Res. Atmos.*, **125**, e2019JD032345, https://doi.org/10.1029/2019JD032345.

Baldwin, M. P., and Coauthors, 2021: Sudden stratospheric warmings. *Rev. Geophys.*, **59**, e2020RG000708, https://doi.org/10.1029/2020RG000708.

Barnes, E. A., and J. A. Screen, 2015: The impact of Arctic warming on the midlatitude jetstream: Can it? Has it? Will it? *Wiley Interdiscip. Rev.: Climate Change*, **6**, 277–286, https://doi.org/10.1002/wcc.337.

Blackport, R., and J. A. Screen, 2019: Influence of Arctic sea ice loss in autumn compared to that in winter on the atmospheric circulation. *Geophys. Res. Lett.*, **46**, 2213–2221, https://doi.org/10.1029/2018GL081469.

——, and ——, 2020: Weakened evidence for mid-latitude impacts of Arctic warming. *Nat. Climate Change*, **10**, 1065–1666, https://doi.org/10.1038/s41558-020-00954-y.

——, ——, K. van der Wiel, and R. Bintanja, 2019: Minimal influence of reduced Arctic sea ice on coincident cold winters in mid-latitudes. *Nat. Climate Change*, **9**, 697–704, https://doi.org/10.1038/s41558-019-0551-4.

Butler, A. H., J. P. Sjoberg, D. J. Seidel, and K. H. Rosenlof, 2017: A sudden stratospheric warming compendium. *Earth Syst. Sci. Data*, **9**, 63–76, https://doi.org/10.5194/essd-9-63-2017.

Cai, D., M. Dameris, H. Garny, and T. Runde, 2012: Implications of all season Arctic sea-ice anomalies on the stratosphere. *Atmos. Chem. Phys.*, **12**, 11 819–11 831, https://doi.org/10.5194/acp-12-11819-2012.

Cohen, J., 2016: An observational analysis: Tropical relative to Arctic influence on midlatitude weather in the era of Arctic amplification. *Geophys. Res. Lett.*, **43**, 5287–5294, https://doi.org/10.1002/2016GL069102.

——, J. Jones, J. C. Furtado, and E. Tziperman, 2013: Warm Arctic, cold continents: A common pattern related to Arctic sea ice melt, snow advance, and extreme winter weather. *Oceanography*, **26**, 150–160, https://doi.org/10.5670/oceanog.2013.70.

——, and Coauthors, 2020: Divergent consensuses on Arctic amplification influence on midlatitude severe winter weather. *Nat. Climate Change*, **10**, 20–29, https://doi.org/10.1038/s41558-019-0662-y.

Dai, A., and M. Song, 2020: Little influence of Arctic amplification on mid-latitude climate. *Nat. Climate Change*, **10**, 231–237, https://doi.org/10.1038/s41558-020-0694-3.

Danabasoglu, G., and Coauthors, 2020: The Community Earth System Model version 2 (CESM2). *J. Adv. Model. Earth Syst.*, **12**, e2019MS001916, https://doi.org/10.1029/2019MS001916.

Deser, C., G. Magnusdottir, R. Saravanan, and A. Phillips, 2004: The effects of North Atlantic SST and sea-ice anomalies on the winter circulation in CCM3. Part II: Direct and indirect components of the response. *J. Climate*, **17**, 877–889, https://doi.org/10.1175/1520-0442(2004)017<0877:TEONAS>2.0.CO;2.

——, R. A. Tomas, M. A. Alexander, and D. Lawrence, 2010: The seasonal atmospheric response to projected Arctic sea ice loss in the late twenty-first century. *J. Climate*, **23**, 333–351, https://doi.org/10.1175/2009JCLI3053.1.

——, ——, and L. Sun, 2015: The role of ocean–atmosphere coupling in the zonal-mean atmospheric response to Arctic sea ice loss. *J. Climate*, **28**, 2168–2186, https://doi.org/10.1175/JCLI-D-14-00325.1.

——, L. Sun, R. A. Tomas, and J. Screen, 2016: Does ocean coupling matter for the northern extratropical response to projected Arctic sea ice loss? *Geophys. Res. Lett.*, **43**, 2149–2157, https://doi.org/10.1002/2016GL067792.

——, J. W. Hurrell, and A. S. Phillips, 2017: The role of the North Atlantic Oscillation in European climate projections. *Climate Dyn.*, **49**, 3141–3157, https://doi.org/10.1007/s00382-016-3502-z.

——, and Coauthors, 2020: Insights from Earth system model initial-condition large ensembles and future prospects. *Nat. Climate Change*, **10**, 277–286, https://doi.org/10.1038/s41558-020-0731-2.

England, M., L. Polvani, and L. Sun, 2018: Contrasting the Antarctic and Arctic atmospheric responses to projected sea ice loss in the late twenty-first century. *J. Climate*, **31**, 6353–6370, https://doi.org/10.1175/JCLI-D-17-0666.1.

Esler, J. G., and R. K. Scott, 2005: Excitation of transient Rossby waves on the stratospheric polar vortex and the barotropic sudden warming. *J. Atmos. Sci.*, **62**, 3661–3682, https://doi.org/10.1175/JAS3557.1.

Fetterer, F., K. Knowles, W. N. Meier, M. Savoie, and A. K. Windnagel, 2017: Sea ice index, version 3 [sea ice extent]. National Snow and Ice Data Center, accessed 16 July 2021, https://doi.org/10.7265/N5K072F8.

Flato, G., and Coauthors, 2013: Evaluation of climate models. *Climate Change 2013: The Physical Science Basis.* T. F. Stocker et al., Eds., Cambridge University Press, 741–866.

Fletcher, C. G., and P. J. Kushner, 2011: The role of linear interference in the annular mode response to tropical SST forcing. *J. Climate*, **24**, 778–794, https://doi.org/10.1175/2010JCLI3735.1.

Francis, J. A., and S. J. Vavrus, 2012: Evidence linking Arctic amplification to extreme weather in mid-latitudes. *Geophys. Res. Lett.*, **39**, L06801, https://doi.org/10.1029/2012GL051000.

Garfinkel, C. I., D. L. Hartmann, and F. Sassi, 2010: Tropospheric precursors of anomalous Northern Hemisphere stratospheric polar vortices. *J. Climate*, **23**, 3282–3299, https://doi.org/10.1175/2010JCLI3010.1.

Hausfather, Z., 2020: Analysis: When might the world exceed 1.5°C and 2°C of global warming? World Economy Forum, accessed 2 June 2021, https://www.weforum.org/agenda/2020/12/analysis-world-paris-agreement-climate-targets-change-emissions-global-warming/.

Haustein, K., M. R. Allen, P. M. Forster, F. E. L. Otto, D. M. Mitchell, H. D. Matthews, and D. J. Frame, 2017: A real-time global warming index. *Sci. Rep.*, **7**, 15417, https://doi.org/10.1038/s41598-017-14828-5.

Hay, S., P. Kushner, R. Blackport, and K. McCusker, 2018: On the relative robustness of the atmospheric circulation response to high-latitude and low-latitude warming. *Geophys. Res. Lett*, https://doi.org/10.1029/2018GL077294.

——, and Coauthors, 2022: Separating the influences of low-latitude warming and sea-ice loss on Northern Hemisphere climate change. *J. Climate*, **35**, 2327–2349, https://doi.org/10.1175/JCLI-D-21-0180.1.

Hurrell, J. W., 1995: Decadal trends in the North Atlantic Oscillation: Regional temperatures and precipitation. *Science*, **269**, 676–679, https://doi.org/10.1126/science.269.5224.676.

——, J. J. Hack, D. Shea, J. M. Caron, and J. Rosinski, 2008: A new sea surface temperature and sea ice boundary dataset for the Community Atmosphere Model. *J. Climate*, **21**, 5145–5153, https://doi.org/10.1175/2008JCLI2292.1.

Jaiser, R., K. Dethloff, and D. Handorf, 2013: Stratospheric response to Arctic sea ice retreat and associated planetary wave propagation changes. *Tellus*, **65A**, 19375, https://doi.org/10.3402/tellusa.v65i0.19375.

——, T. Nakamura, D. Handorf, K. Dethloff, J. Ukita, and K. Yamazaki, 2016: Atmospheric winter response to Arctic sea ice changes in reanalysis data and model simulations. *J. Geophys. Res. Atmos.*, **121**, 7564–7577, https://doi.org/10.1002/2015JD024679.

Kalnay, E., and Coauthors, 1996: The NCEP/NCAR 40-Year Reanalysis Project. *Bull. Amer. Meteor. Soc.*, **77**, 437–472, https://doi.org/10.1175/1520-0477(1996)077<0437:TNYRP>2.0.CO;2.

Kay, J. E., and Coauthors, 2015: The Community Earth System Model (CESM) large ensemble project: A community resource for studying climate change in the presence of internal climate variability. *Bull. Amer. Meteor. Soc.*, **96**, 1333–1349, https://doi.org/10.1175/BAMS-D-13-00255.1.

Kim, B.-M., S.-W. Son, S.-K. Min, J.-H. Jeong, S.-J. Kim, X. Zhang, T. Shim, and J.-H. Yoon, 2014: Weakening of the stratospheric polar vortex by Arctic sea-ice loss. *Nat. Commun.*, **5**, 4646, https://doi.org/10.1038/ncomms5646.

Kolstad, E. W., and J. A. Screen, 2019: Nonstationary relationship between autumn Arctic sea ice and the winter North Atlantic Oscillation. *Geophys. Res. Lett.*, **46**, 7583–7591, https://doi.org/10.1029/2019GL083059.

Kretschmer, M., and Coauthors, 2018: 2018: More frequent weak stratospheric polar vortex states linked to mid-latitude cold extremes. *Bull. Amer. Meteor. Soc.*, **99**, 49–60, https://doi.org/10.1175/BAMS-D-16-0259.1.

Labe, Z. M., 2020: The effects of Arctic sea-ice thickness loss and stratospheric variability on mid-latitude cold spells. Doctoral dissertation. University of California, 158 pp., https://escholarship.org/uc/item/778982rr.

——, Y. Peings, and G. Magnusdottir, 2019: The effect of QBO phase on the atmospheric response to projected Arctic sea ice loss in early winter. *Geophys. Res. Lett.*, **46**, 7663–7671, https://doi.org/10.1029/2019GL083095.

Larson, V. E., 2017: CLUBB-SILHS: A parameterization of subgrid variability in the atmosphere. 133 pp., https://arxiv.org/abs/1711.03675.

Liang, Y.-C., and Coauthors, 2020: Quantification of the Arctic sea ice–driven atmospheric circulation variability in coordinated large ensemble simulations. *Geophys. Res. Lett.*, **47**, e2019GL085397, https://doi.org/10.1029/2019GL085397.

Maher, N., and Coauthors, 2019: The Max Planck Institute Grand Ensemble: Enabling the exploration of climate system variability. *J. Adv. Model. Earth Syst.*, **11**, 2050–2069, https://doi.org/10.1029/2019MS001639.

McCusker, K. E., J. C. Fyfe, and M. Sigmond, 2016: Twenty-five winters of unexpected Eurasian cooling unlikely due to Arctic sea ice loss. *Nat. Geosci.*, **9**, 838–842, https://doi.org/10.1038/ngeo2820.

McKenna, C. M., T. J. Bracegirdle, E. F. Shuckburgh, P. H. Haynes, and M. M. Joshi, 2018: Arctic sea ice loss in different regions leads to contrasting Northern Hemisphere impacts. *Geophys. Res. Lett.*, **45**, 945–954, https://doi.org/10.1002/2017GL076433.

Mori, M., M. Watanabe, H. Shiogama, J. Inoue, and M. Kimoto, 2014: Robust Arctic sea-ice influence on the frequent Eurasian cold winters in past decades. *Nat. Geosci.*, **7**, 869–873, https://doi.org/10.1038/ngeo2277.

——, Y. Kosaka, M. Watanabe, H. Nakamura, and M. Kimoto, 2019a: A reconciled estimate of the influence of Arctic sea-ice loss on recent Eurasian cooling. *Nat. Climate Change*, **9**, 123–129, https://doi.org/10.1038/s41558-018-0379-3.

——, and Coauthors, 2019b: Reply to: Is sea-ice-driven Eurasian cooling too weak in models? *Nat. Climate Change*, **9**, 937–939, https://doi.org/10.1038/s41558-019-0636-0.

Mudelsee, M., 2010: *Climate Time Series Analysis: Classical Statistical and Bootstrap Methods.* 1st ed. Springer, 474 pp.

Nakamura, T., K. Yamazaki, K. Iwamoto, M. Honda, Y. Miyoshi, Y. Ogawa, Y. Tomikawa, and J. Ukita, 2016: The stratospheric pathway for Arctic impacts on midlatitude climate. *Geophys. Res. Lett.*, **43**, 3494–3501, https://doi.org/10.1002/2016GL068330.

Notz, D., and Coauthors, 2020: Arctic sea ice in CMIP6. *Geophys. Res. Lett.*, **47**, e2019GL086749, https://doi.org/10.1029/2019GL086749.

Ogawa, F., and Coauthors, 2018: Evaluating impacts of recent Arctic sea ice loss on the Northern Hemisphere winter climate change. *Geophys. Res. Lett.*, **45**, 3255–3263, https://doi.org/10.1002/2017GL076502.

O'Neill, A., and V. D. Pope, 1988: Simulations of linear and nonlinear disturbances in the stratosphere. *Quart. J. Roy. Meteor. Soc.*, **114**, 1063–1110, https://doi.org/10.1002/qj.49711448210.

Overland, J. E., K. R. Wood, and M. Wang, 2011: Warm Arctic-cold continents: Climate impacts of the newly open arctic sea. *Polar Res.*, **30** (Suppl.), 1–14, https://doi.org/10.3402/polar.v30i0.15787.

Peings, Y., 2019: Ural blocking as a driver of early-winter stratospheric warmings. *Geophys. Res. Lett.*, **46**, 5460–5468, https://doi.org/10.1029/2019GL082097.

——, and G. Magnusdottir, 2014: Response of the wintertime Northern Hemisphere atmospheric circulation to current and projected Arctic sea ice decline: A numerical study with CAM5. *J. Climate*, **27**, 244–264, https://doi.org/10.1175/JCLI-D-13-00272.1.

——, Z. M. Labe, and G. Magnusdottir, 2021: Are 100 ensemble members enough to capture the remote atmospheric response to +2°C Arctic sea ice loss? *J. Climate*, **34**, 3751–3769, https://doi.org/10.1175/JCLI-D-20-0613.1.

Perlwitz, J., M. Hoerling, and R. Dole, 2015: Arctic tropospheric warming: Causes and linkages to lower latitudes. *J. Climate*, **28**, 2154–2167, https://doi.org/10.1175/JCLI-D-14-00095.1.

Plumb, R. A., 1981: Instability of the distorted polar night vortex: A theory of stratospheric warmings. *J. Atmos. Sci.*, **38**, 2514–2531, https://doi.org/10.1175/1520-0469(1981)038<2514:IOTDPN>2.0.CO;2.

——, 1985: On the three-dimensional propagation of stationary waves. *J. Atmos. Sci.*, **42**, 217–229, https://doi.org/ 10.1175/1520-0469(1985)042,0217:OTTDPO.2.0.CO;2.

Polvani, L. M., and D. W. Waugh, 2004: Upward wave activity flux as precursor to extreme stratospheric events and subsequent anomalous surface weather regimes. *J. Climate*, **17**, 3548–3554, https://doi.org/10.1175/1520-0442(2004)017<3548:UWAFAA>2.0.CO;2.

——, L. Sun, A. H. Butler, J. H. Richter, and C. Deser, 2017: Distinguishing stratospheric sudden warmings from ENSO as key drivers of wintertime climate variability over the North Atlantic and Eurasia. *J. Climate*, **30**, 1959–1969, https://doi.org/10.1175/JCLI-D-16-0277.1.

Ronalds, B., E. A. Barnes, R. Eade, Y. Peings, and M. Sigmond, 2020: North Pacific zonal wind response to sea ice loss in the Polar Amplification Model Intercomparison Project and its downstream implications. *Climate Dyn.*, **55**, 1779–1792, https://doi.org/10.1007/s00382-020-05352-w.

Ruggieri, P., R. Buizza, and G. Visconti, 2016: On the link between Barents-Kara sea ice variability and European blocking. *J. Geophys. Res. Atmos.*, **121**, 5664–5679, https://doi.org/10.1002/2015JD024021.

Scinocca, J. F., M. C. Reader, D. A. Plummer, M. Sigmond, P. J. Kushner, T. G. Shepherd, and R. Ravishankara, 2009: Impact of sudden Arctic sea-ice loss on stratospheric polar ozone. *Geophys. Res. Lett.*, **36**, L24701, https://doi.org/10.1029/2009GL041239.

Scott, R. K., and D. G. Dritschel, 2006: Vortex–vortex interactions in the winter stratosphere. *J. Atmos. Sci.*, **63**, 726–740, https://doi.org/10.1175/JAS3632.1.

Screen, J. A., 2017: Simulated atmospheric response to regional and pan-Arctic sea ice loss. *J. Climate*, **30**, 3945–3962, https://doi.org/10.1175/JCLI-D-16-0197.1.

——, and I. Simmonds, 2010: The central role of diminishing sea ice in recent Arctic temperature amplification. *Nature*, **464**, 1334–1337, https://doi.org/10.1038/nature09051.

——, and R. Blackport, 2019: Is sea-ice-driven Eurasian cooling too weak in models? *Nat. Climate Change*, **9**, 934–936, https://doi.org/10.1038/s41558-019-0635-1.

——, I. Simmonds, C. Deser, and R. Tomas, 2013: The atmospheric response to three decades of observed Arctic sea ice loss. *J. Climate*, **26**, 1230–1248, https://doi.org/10.1175/JCLI-D-12-00063.1.

——, C. Deser, I. Simmonds, and R. Tomas, 2014: Atmospheric impacts of Arctic sea-ice loss, 1979–2009: Separating forced change from atmospheric internal variability. *Climate Dyn.*, **43**, 333–344, https://doi.org/10.1007/s00382-013-1830-9.

——, and Coauthors, 2018: Consistency and discrepancy in the atmospheric response to Arctic sea ice loss across climate models. *Nat. Geosci.*, **11**, 155–163, https://doi.org/10.1038/s41561-018-0059-y.

Seviour, W. J. M., 2017: Weakening and shift of the Arctic stratospheric polar vortex: Internal variability or forced response? *Geophys. Res. Lett.*, **44**, 3365–3373, https://doi.org/10.1002/2017GL073071.

Sigmond, M., and J. F. Scinocca, 2010: The influence of basic state on the Northern Hemisphere circulation response to climate change. *J. Climate*, **23**, 1434–1446, https://doi.org/10.1175/2009JCLI3167.1.

——, ——, V. V. Kharin, and T. G. Shepherd, 2013: Enhanced seasonal forecast skill following stratospheric sudden warmings. *Nat. Geosci.*, **6**, 98–102, https://doi.org/10.1038/ngeo1698.

Simpson, I. R., and Coauthors, 2020: An evaluation of the large-scale atmospheric circulation and its variability in CESM2 and other CMIP models. *J. Geophys. Res. Atmos.*, **125**, e2020JD032835, https://doi.org/10.1029/2020JD032835.

Smith, D. M., N. J. Dunstone, A. A. Scaife, E. K. Fiedler, D. Copsey, and S. C. Hardiman, 2017: Atmospheric response to Arctic and Antarctic sea ice: The importance of ocean–atmosphere coupling and the background state. *J. Climate*, **30**, 4547–4565, https://doi.org/10.1175/JCLI-D-16-0564.1.

——, and Coauthors, 2019: The Polar Amplification Model Intercomparison Project (PAMIP) contribution to CMIP6: Investigating the causes and consequences of polar amplification. *Geosci. Model Dev.*, **12**, 1139–1164, https://doi.org/10.5194/gmd-12-1139-2019.

——, and Coauthors, 2020: North Atlantic climate far more predictable than models imply. *Nature*, **583**, 796–800, https://doi.org/10.1038/s41586-020-2525-0.

——, and Coauthors, 2022: Robust but weak winter atmospheric circulation response to future Arctic sea ice loss. *Nat. Commun.*, **13**, 727, https://doi.org/10.1038/s41467-022-28283-y.

Smith, K. L., and P. J. Kushner, 2012: Linear interference and the initiation of extratropical stratosphere–troposphere interactions. *J. Geophys. Res.*, **117**, D13107, https://doi.org/10.1029/2012JD017587.

Streffing, J., T. Semmler, L. Zampieri, and T. Jung, 2021: Response of Northern Hemisphere weather and climate to Arctic Sea ice decline: Resolution independence in Polar Amplification Model Intercomparison Project (PAMIP) simulations. *J. Climate*, **34**, 8445–8457, https://doi.org/10.1175/JCLI-D-19-1005.1.

Sun, L., C. Deser, L. M. Polvani, and R. Tomas, 2014: Influence of projected Arctic sea ice loss on polar stratospheric ozone and circulation in spring. *Environ. Res. Lett.*, **9**, 084016, https://doi.org/10.1088/1748-9326/9/8/084016.

——, —— and R. A. Tomas, 2015: Mechanisms of stratospheric and tropospheric circulation response to projected Arctic sea ice loss. *J. Climate*, **28**, 7824–7845, https://doi.org/10.1175/JCLI-D-15-0169.1.

——, J. Perlwitz, and M. Hoerling, 2016: What caused the recent "warm Arctic, cold continents" trend pattern in winter temperatures? *Geophys. Res. Lett.*, **43**, 5345–5352, https://doi.org/10.1002/2016GL069024.

——, M. A. Alexander, and C. Deser, 2018: Evolution of the global coupled climate response to Arctic sea ice loss during 1990–2090 and its contribution to climate change. *J. Climate*, **31**, 7823–7843, https://doi.org/10.1175/JCLI-D-18-0134.1.

Thompson, D. W. J., and J. M. Wallace, 2000: Annular modes in the extratropical circulation. Part I: Month-to-month variability. *J. Climate*, **13**, 1000–1016, https://doi.org/10.1175/1520-0442(2000)013<1000:AMITEC>2.0.CO;2.

——, E. A. Barnes, C. Deser, W. E. Foust, and A. S. Phillips, 2015: Quantifying the role of internal climate variability in future climate trends. *J. Climate*, **28**, 6443–6456, https://doi.org/10.1175/JCLI-D-14-00830.1.

Tomas, R. A., C. Deser, and L. Sun, 2016: The role of ocean heat transport in the global climate response to projected Arctic sea ice loss. *J. Climate*, **29**, 6841–6859, https://doi.org/10.1175/JCLI-D-15-0651.1.

Tung, K.-K., and R. S. Lindzen, 1979: A theory of stationary long waves. Part I: A simple theory of blocking. *Mon. Wea. Rev.*, **107**, 714–734, https://doi.org/10.1175/1520-0493(1979)107<0714:ATOSLW>2.0.CO;2.

Wang, K., C. Deser, L. Sun, and R. Tomas, 2018: Fast response of the tropics to an abrupt loss of Arctic sea ice via ocean dynamics. *Geophys. Res. Lett.*, **45**, 4264–4272, https://doi.org/10.1029/2018GL077325.

Warner, J. L., J. A. Screen, and A. A. Scaife, 2020: Links between Barents-Kara sea ice and the extratropical atmospheric circulation explained by internal variability and tropical forcing. *Geophys. Res. Lett.*, **47**, e2019GL085679, https://doi.org/10.1029/2019GL085679.

Wilks, D. S., 2016: "The stippling shows statistically significant grid points": How research results are routinely overstated and overinterpreted, and what to do about it. *Bull. Amer. Meteor. Soc.*, **97**, 2263–2273, https://doi.org/10.1175/BAMS-D-15-00267.1.

Wu, Y., and K. L. Smith, 2016: Response of Northern Hemisphere midlatitude circulation to Arctic amplification in a simple atmospheric general circulation model. *J. Climate*, **29**, 2041–2058, https://doi.org/10.1175/JCLI-D-15-0602.1.

Zhang, P., Y. Wu, and K. L. Smith, 2017: Prolonged effect of the stratospheric pathway in linking Barents-Kara Sea ice variability to the midlatitude circulation in a simplified model. *Climate Dyn.*, **50**, 527–539, https://doi.org/10.1007/s00382-017-3624-y.

——, ——, I. R. Simpson, K. L. Smith, X. Zhang, B. De, and P. Callaghan, 2018: A stratospheric pathway linking a colder Siberia to Barents-Kara Sea ice loss. *Sci. Adv.*, **4**, eaat6025, https://doi.org/10.1126/sciadv.aat6025.